NTNU – Trondheim
Norwegian University of
Science and Technology

Pneumatic Components and Alumina Feeding Equipment HAL4e

Simen Vatslid Øystese

Master of Science in Mechanical Engineering
Submission date: June 2015
Supervisor: Knut Sørby, IPK
Co-supervisor: Anders Lilleby, Norsk Hydro

Norwegian University of Science and Technology
Department of Production and Quality Engineering

Pneumatic Components and Alumina Feeding Equipment HAL4e

Stud.Techn. Simen Vatslid Øystese

June 2015

M.Sc Thesis
TPK 4940 - Production Technology
Department of Production and Quality Engineering
Norwegian University of Science and Technology

Supervisor 1: Professor Knut Sørby, NTNU
Supervisor 2: Dr. Anders Lilleby, Hydro

Preface

The work presented here is a M.Sc. Thesis carried out at the department of Production and Quality Engineering at the Norwegian University of Science and Technology (NTNU). The thesis was carried out during the the spring semester of 2015 and represents the concluding work of a five year M.Sc. degree in Mechanical Engineering.

The task for this thesis was given by Norsk Hydro and the experiments have been carried out at Hydro's lead research center located in Årdal, Norway. The results have a direct link to the Primary Aluminium production and is focused on the next generation production plant technology.

Simen V. Øystese

Trondheim, 2015-06

Acknowledgment

As main supervisor and professor for many years I would like to give special thanks to Professor Knut Sørby for his help and support not only during this thesis but throughout my studies.

The task was created by Dr. Anders Lilleby who has, as my primary contact in Norsk Hydro and external supervisor provided great input and help throughout the completion of this thesis.

I have also been very lucky to work with and discuss my results with Hydro's lead researches in the field of fluidised transport, Dr. Are Dyrøy, Dr. Morten Karlsen and PhD Candidate Serena Carmen Valciu, who's contributions are highly valued and appreciated.

Additionally, I have to acknowledge Øystein Vigdal for his help with retrofitting of the test rig, and the rest of the Primary Metal Technlology (PMT) department of Hydro Årdal.

S. V. Ø.

Abstract

This thesis presents the current design variations and possible solutions for optimisation of the alumina distribution system for the next generation aluminium production cell. The alumina distribution system is of high importance to the production system, as alumina is the raw material in the primary aluminium production. The new cells (HAL4e) are currently operating as six cells in Hydro Årdal with a planned expansion to a 60 cell pilot plant in Hydro Karmøy, 2017. This thesis investigates the distribution of alumina over the cell length of the cell air slide, and the actual feeding of alumina through eight point feeders distributed along cell length.

The alumina transportation is done by fluidisation of alumina, which in short gives the alumina a fluid like behaviour and utilises the fluid head for transportation. Fluidisation is, however, not a binary effect which means that the transportation capacity is dependent on the air velocity used for fluidisation and not only if the velocity is sufficient to reach a fluidised state.

Simulations indicate that a small supply tube for compressed air could lead to a large pressure drop along the cell length for the cell air slide. Specifically this means that an inner diameter of 12 mm, as is present on the L24 and L25 cells, leads to an unstable fluidisation. The optimal design as of today is the Ø15 mm inner diameter pipe used on cell L26 and L27. With the current nozzles, this provides a relatively stable fluidisation velocity despite the small pressure drop. This also leads to a 6 % reduction in consumption compared to the L22 and L23 design that is equipped with a Ø19 mm inner diameter supply tube.

The pressure drop on the L26/L27 design is, however, a factor in the optimisation of the cell air slide. A solution that could lead to a 19 % reduction in consumption is a pressure reduction to 5.5 bar absolute pressure on the air supply. The Ø19 mm supply is in this case optimal due to the marginal pressure drop over the cell length. Measurements carried out as part of this thesis also indicate that the fluidising velocity at 5.5 bar absolute pressure is sufficient to achieve desired transport capacity.

The air consumption is, however, of minor importance on the point feeders due to the marginal flow in the elements. In this case, the important factor is the accuracy of doses, which in this thesis is shown to increase with reducing pressure based on measurements carried out at a test rig in Årdal.

As the cell air slide has a higher requirement to the air pressure than the feeders, and since the feeders show improved results for pressure below this limit, implementation of two separate pressure regulators is recommended.

This thesis also suggests a change in the operation of the point feeders. The point feeders are currently operated with a control volume being emptied each cycle. The reduced standard deviation in the doses at 3.0 barg could allow the feeders to operate without this control volume. This way the end effects of each cycle could also be eliminated. Even though this leads to reliable doses, the removal of the control volume still causes a slight increase in standard deviation over time. The increase is small and this thesis, therefore, concludes that a re-evaluation of the operational parameters should be considered.

In general, this thesis concludes that a pressure reduction on the fluidised transportation system is a good solution to increase accuracy and reduce consumption. Further testing in the actual production is, however, required before large-scale implementation.

Sammendrag

Denne masteroppgaven presenterer de ulike designvariasjonene og muligheter for optimalisering av matesystemet for alumina i neste generasjons produksjonscelle for aluminium. Matesystemet er spesielt viktig for produksjonssystemet, da alumina er råmaterialet for aluminiumsproduksjonen. De nye cellene (HAL4e) opererer for øyeblikket ved Hydro Aluminium Årdal bestående av seks celler, med en planlagt ekspansjon i 2017 til 60 celler ved Hydro Karmøy. Denne oppgaven ser nærmere på distribusjonssystemet i hver enkelt celle. Dette innebærer en alumina luftrenne for distribusjon over cellens lengde og de åtte mateapparatene som er fordelt utover på cellen.

Transporten av alumina gjøres ved hjelp av fluidisering som innebærer at trykkluft blåses gjennom pulveret slik at det får fluidliknende oppførsel. Pulveret kan i denne tilstanden transporteres ved hjelp av en liten helning. Det er likevel viktig å bemerke at fluidisert transport ikke bare er avhengig av om pulveret er fluidisert eller ikke, men at viskositeten, og dermed transportkapasiteten endres ved lufthastigheten gjennom pulveret.

Simuleringer indikerer at diameteren på tilløpsrøret for trykkluft er svært viktig for luftrennen da en liten diameter fører til et stort trykktap over cellens lengde. Dette betyr at designet som nå opererer på cellene L24 og L25 med indre diameter på 12 mm fører til en ustabil fluidisering. Det optimale designet per dags dato er med Ø15 mm tilløp som opererer på celle L26 og L27. Her er der fortsatt et trykktap i forhold til L22 og L23 med 19 mm tilløp men det er ikke stort nok til å utgjøre noen forskjell for dagens produksjon. Reduksjonen i indre diameter leder på den andre siden til en luftbesparelse på 6 % som er bakgrunn for denne avgjørelsen.

For optimalisering av prosessen er det derimot funnet at en trykkreduksjon fra 7.0 til 5.5 bar absolutt trykk gir en luftbesparelse på 19 %. Ved reduksjon i tykk er det designet med 19 mm tilløp som er valgt, da det å presse prosessen medfører høyere krav til stabilitet. Forsøk gjennonført i sammenheng med denne oppgaven viser også at transportkapasiteten ved dette trykket er tilstrekkelig i forhold til gjeldende operasjonsparametere.

Når det gjelder punktmaterne er luftbesparelse derimot mindre viktig, da forbruket i utgangspunktet er lavt. Det sentrale er derfor å øke nøyaktigheten i apparatenes doser, som basert på resultatene i denne oppgaven kan gjøres ved trykkreduksjon.

I og med at luftrennen har høyere krav til trykk enn mateapparatene, og at mateapparatene viser forbedrede resultater også under dette begrensende trykket er det derfor anbefalt med to regulatorer per celle.

I tillegg til dette anbefaler denne oppgaven også en reevaluering av hvordan mateapparatene blir operert. I dag opereres apparatene med et kontrollvolum som skal forsikre at mengden alumina gitt i hver syklus er stabil. Dette medfører derimot store avvik i dosestørrelse mot slutten av denne syklusen. Resultater i denne oppgaven tilsier at standardavviket på dosene er lavt nok ved 3.0 barg, slik at operasjon uten bruk av kontrollvolum ikke medfører signifikant økning i avvik over tid.

Reduksjon av trykk i det fluidiserte transportsystemet er derfor en god løsning for både reduksjon av forbruk og økt nøyaktighet. Videre testing i større skala er derimot nødvendig før implementering av trykkregulatorer.

Contents

List of Figures

List of Tables

Chapter 1

Introduction

1.1 Introduction to Aluminium Electrolysis

To understand the relevance of this thesis it is important to first establish an overview of a few basic concepts related to aluminium production. This section will, therefore, first provide the necessary background required to understand the main principles and challenges in this thesis.

1.1.1 The Production Cell

The aluminium production is a relatively simple concept and is based on the Hall-Heroult prebake technology. A general overview is that carbon anodes are placed in a cryolyte bath containing dissolved alumina. This reactor containing several anodes is illustrated with a simplified cross section in Figure 1.1 and is commonly referred to as the cell or pot which are the terms that will be used throughout this thesis.

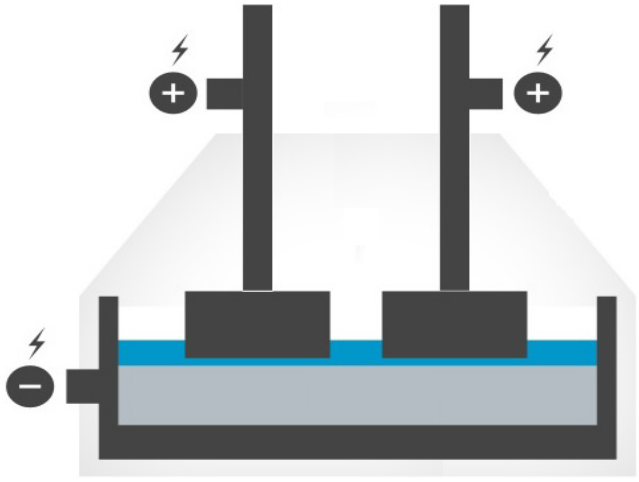

Figure 1.1: Simplified cross section of an aluminium production cell (Source: Hydro.com)

An aluminium plant consists of several of these cells forming a pot line that produce aluminium continuously. The actual production is basic electrolysis where power is supplied to produce aluminium from alumina. The alumina is dissolved in the cryolyte bath to reduce its melting point and there are also other additives in the bath to improve production quality. This study does, however, not focus on the complex bath composition and the simplified overall equation of the process is as follows in Equation 1.1.

$$2Al_2O_{3(s)} + 3C_{(s)} \rightarrow 4Al_{(l)} + 3CO_{2(g)} \tag{1.1}$$

The pure aluminium sinks to the bottom of the cells and can be tapped as a pure liquid regularly, while anodes have to be replaced throughout the pot life [1].

1.1.2 Alumina Distribution

Alumina is, as previously mentioned, the main raw material for aluminium production and a it is consumed in a ratio of 1.89 kg Al_2O_3 per 1.00 kg Al. To maintain production it is crucial that the bath has a sufficient concentration of alumina and a reliable distribution system is, therefore, very important for the process.

In older technologies the alumina were fed in large additions and the bath concentration, therefore, had high variations. The cell voltage is, however, very dependent on the alumina concentration in the bath. As seen in Figure 1.2 the cell voltage is at a minimum with an alumina concentration of 3-5 mass %. A normal cell does, however, operate in the area 2-5 % as the exponential rise in cell voltage is used as a control parameter [2] [3] [1].

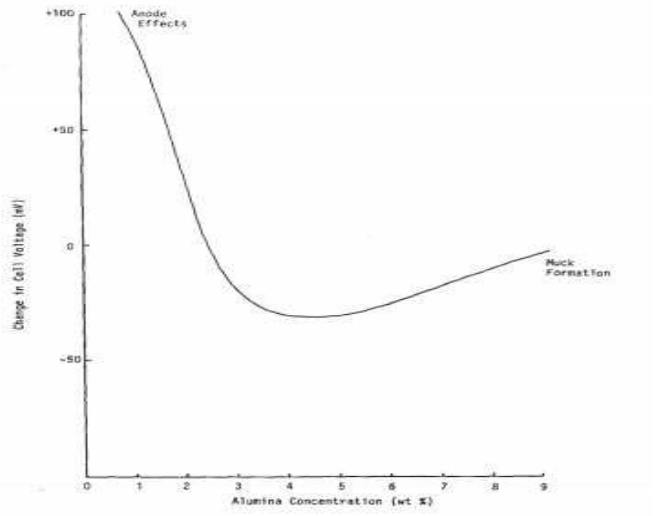

Figure 1.2: Cell voltage and alumina concentration relationship [3]

In Figure 1.2 there is also listed sludge and anode effect at the end points of the graph. The anode effect occurs when the alumina concentration is so low that the bath is non-conductive and thus inhibiting the production. Sludge formation does on the other hand happen when the bath is saturated with alumina. In this case the excess alumina sinks to the bottom of the

cell forming a non-conductive layer that can be difficult to remove. Sludge formation does, however, not necessarily mean that the whole pot is saturated. Large additions of alumina could lead to local saturation at the feeding point and sludge could, therefore, form with a low average concentration in the cell. Maintaining a stable concentration of alumina throughout the cell is, therefore, of high importance and the doses should be small enough to allow all of the alumina to dissolve before sinking to the bottom.

Based on this theory, modern aluminium production cells are equipped with several feeding points throughout the cell operating with small doses between 400 g and 1.2 kg. This did, however, lead to a higher wear on the feeding equipment due to the high number of cycles and mechanical components required increased maintenance [4].

The feeding equipment in the HAL4e technology is, therefore, based the principle of fluidisation and operates without moving parts and thus, a very low need for maintenance. The aerated distribution system (ADS) and the principles of fluidisation will be explained in full in the next chapter but the basic concept is that compressed air is used to fluidise the solid alumina powder. This means that the alumina obtains a fluid-like behaviour and the hydrostatic head is utilised to distribute the alumina.

1.2 Intention and Industrial Relevance

The fluidised transport does on the other hand have a main limitation. The previous mechanical systems were able to provide a higher accuracy on the doses compared to the fluidised feeding system that has a higher variation in dose size.

Based on the low maintenance requirement offered by the fluidised system it has, however, been chosen as the future technology to be implemented in the new pilot plant at Karmøy to be built 2017. The plant will consist of 60 pilot cells of which 48 will be the HAL4e technology currently being tested in Hydros test center in Årdal. The intention of this thesis is to evaluate the current status of the feeding system on the six HAL4e cells operating in Årdal and investigate options for improving the feeding accuracy and reducing the consumption of compressed air.

This thesis will, therefore, provide an overview of the current feeding system based on actual measurements calculations and simulations. Options for improvements will also be investigated with the intention of being able to provide an improved design suggestion to the Karmøy large scale pilot plant.

This thesis will also explain several principles related to the fluidisation of alumina. Even though the thesis will give an overview of these principles it does not have a great focus on the actual powder technology related to fluidisation. This thesis is as explained focused on improving the mechanical design of the alumina feeding system to improve its functionality.

Chapter 2

Background

2.1 Aerated Distribution System (ADS) HAL4e

As previously mentioned the alumina distribution is a vital part of any electrolysis cell and there has been several ways of transportation of alumina over the years. The HAL4e cells are developed with an aerated distribution system (ADS) which utilises the principle of particle fluidisation to transport alumina from silo to cell. This system consists of inclined conveyer boxes equipped with several aeration elements that fluidise the alumina and thus utilising the head of the fluidised alumina for transport.

The main benefit of the ADS is the low need for maintenance compared to traditional systems. The aerated distribution system consists mostly of rigid parts and with valves placed at a distance from the cell the exposed areas are reduced to a minimum. However, due to the hardness of alumina, not only movable parts are critical as the alumina will act as a sandblaster when conveyed at high speed. The low velocity distribution offered by the ADS is, therefore, also a great benefit. A practical example is that the ADS system on 28 cells in Karmøy, Norway has operated with no need for maintenance since installation in 1996.[4] There have, however, been some deviations and alterations over the years but this is mainly due to it being the first full scale testing of the system.

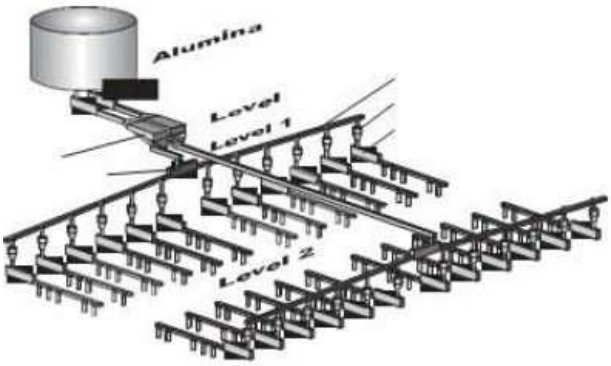

Figure 2.1: Figure illustrating the layout and the three levels of the ADS [4]

The ADS system could be divided into 3 levels as seen in Figure 2.1. The first level, level 0, is

defined as the conveyor from the silo and into the pot room. The next level is inside the pot room distributing to a dedicated control volume for each cell. Level 2 is the main focus of this report and is the final part of the system, distributing alumina into the electrolysis cell. [5]

2.1.1 Cell Air Slide

Earlier a brief presentation of the ADS was given, this project is, however, focused on the last part of the distribution system where the alumina is delivered from pot room wall to the cell. The two vital parts of this operation is the cell air slide and the point feeders that are shown in Figure 2.2.

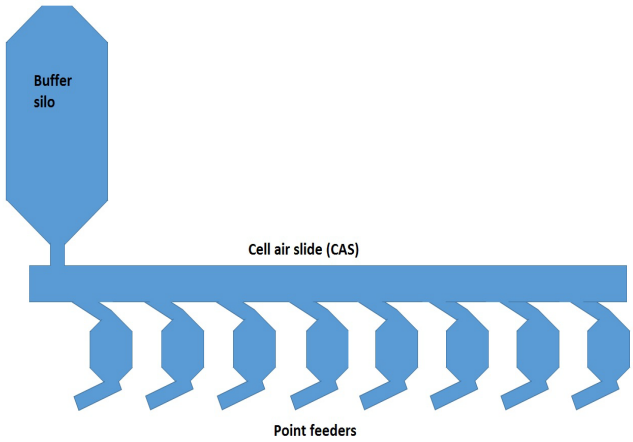

Figure 2.2: Illustration of the alumina air slide and point feeders

The cell air slide lies on top of the cell with a 1 degree inclination and is equipped with several fluidisation elements that distribute air below the solid alumina bed base. The activation of these elements cause the alumina to enter a fluid-like state and flow freely along the cell air slide until a steady state level, which will be addressed at a later point, is achieved.

The fluidisation of alumina in the cell air slide is, however, dependent on all the elements being functional. If one element should be blocked or for some reason unable to supply enough air this element would block transportation as the alumina will in this section remain in solid state.

2.1.2 Point Feeders

The point feeders operate on the same fluidisation principle as the cell air slide. The point feeders do, however, operate with two small elements feeding to and from a control volume. There are some variations on the size of the control volume and the length of the elements but this will be addressed at a later point in this thesis.

The main idea is that the point feeders supply the cell with alumina in doses between 400g and 1.2 kg. As mentioned, the optimal dose is in theory as small as possible. However, there

are other limiting factors that demands a larger dose size. The most important factor is the breakers operating with each point feeder. In the aluminium production process the cryolyte freeze and form a hard layer on top of the bath. To be able to supply alumina to the bath the breakers are, therefore, crucial. They break hole in the crust and allow alumina to be distributed into the bath. The use of very small doses does require a higher number of cycles on the breakers and the wear has to be taken into account when setting a desired dose.

Throughout this report the calculations will be based on doses around 900 g. The results will, however, be applicable for all dose settings as this report in focused on increasing the dose accuracy and reducing the air consumption in the aerated distribution system.

2.2 Principles of Fluidisation

The main principle of fluidisation is to bring solid particles to a fluidised state by the use of a fluid, either gas or liquid [6]. This research is based on the use of fluidisation in the aluminium industry, where compressed air is used to fluidise alumina powder.

Fluidisation occurs when a fluid, being either liquid or gas is distributed so that it ascends through a bed of particles. Passing through the bed of solid particles the fluid exerts a drag force bringing the particles to a loose state. The fluid behaviour is obtained when the drag and buoyancy forces exceeds the gravitational forces of the solid particles as shown in Figure 2.3. [7]

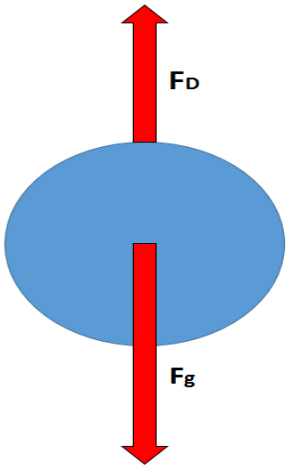

Figure 2.3: Illustration of the drag and gravitational forces acting on the solid particles

The fluidised bed is the name of the reactor where the fluidisation takes place and even though there are several different variations of fluidised beds, most of them operate on a similar principle and with some key components. These are the plenum where the fluid enters the bed and the distributor where the fluid is evenly distributed under the bed base. The compressed air flows upwards through fluidisation elements where the air is distributed with a even velocity over the entire bed base. These fluidisation elements are, therefore, made up of a porous membrane over a nozzle for air supply as shown in Figure 2.4.

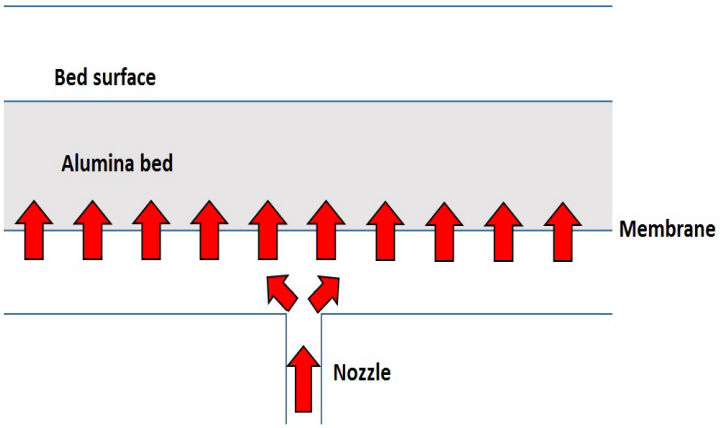

Figure 2.4: Illustration alumina fluidisation on the elements inside the cell air slide

2.2.1 Flow Regimes

The fluidisation of powder can according to Crowe (2003) [8] be divided into six regimes that define different degrees of fluidisation as shown in Figure 2.5. The first defined regime is the fixed bed. Here the velocity of the air passing through the solid is too low to move the particles and the solid, therefore, remains stationary. As the velocity increases the bed reaches a bubbling regime. In this regime the air begins to form bubbles in the solid particles. This regime is easily detected by observation of the bed surface and is a clear indicator that the material has obtained fluid-like properties.

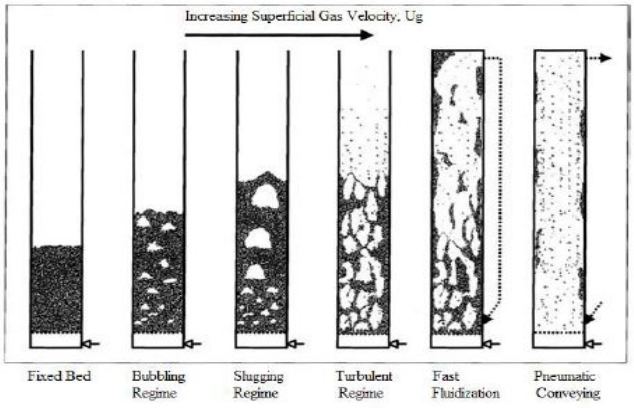

Figure 2.5: Fluidisation regimes in fluidised beds [8]

The next regime shown in the figure is also bubbling, however, the slugging regime appears when the bubbles start to form bubbles larger than 2/3 of the bed diameter. These large bubbles only occurs when the bed height to diameter ratio exceeds 2, ($\frac{h}{D} > 2$) and the smaller

bubbles have time to combine into larger ones. Due to the uneven fluidisation of the solids, it is preferred to keep a low height to diameter ratio so that this regime can be avoided.

Increasing the fluidisation velocity even more leads to the next three regimes of fluidisation. One thing in common for all three of them is that the alumina surface no longer is easy to define. The turbulent regime occurs when the fluidising velocity is so high that the bubbles collapse. This leads to a turbulent behaviour in the whole distribution slide and the powder handling becomes less controllable. [7]

In both the fast fluidisation and pneumatic conveying regime the air velocity is high enough to transport solid out of the system. The fast fluidisation regime can be seen when the ventilated air can carry solid particles out of the system. In pneumatic conveying the whole bed enters a dilute phase and even more solids are transported out as exhaust.

2.2.2 Powder Classification

The hydrodynamic behaviour of the solid depends on the particle diameter and density. Geldart (1973) [9] used four categories to classify the powders based on their behavior in fluidisation. The categories A (Aeratable), B (Sandlike), C (Cohesive) and D (Spoutable) are defined based on particle diameter and particle density and can be seen in the Geldart diagram in Figure 2.6.

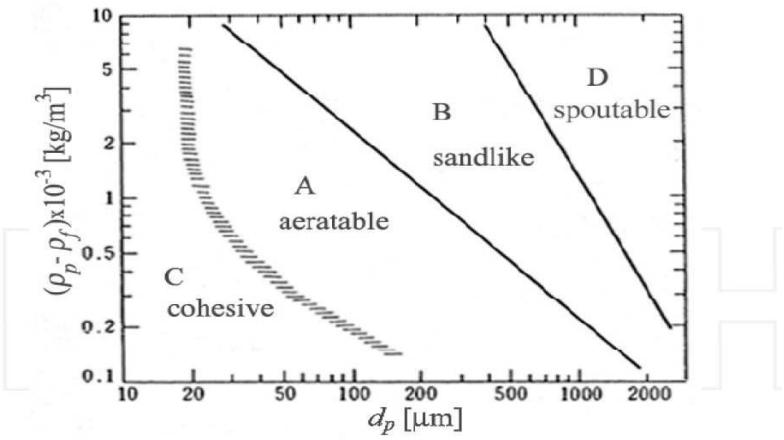

Figure 2.6: Geldarts powder classification diagram [10]

Figure 2.7 illustrates how these powders behave according to the fluidisation regimes explained earlier.

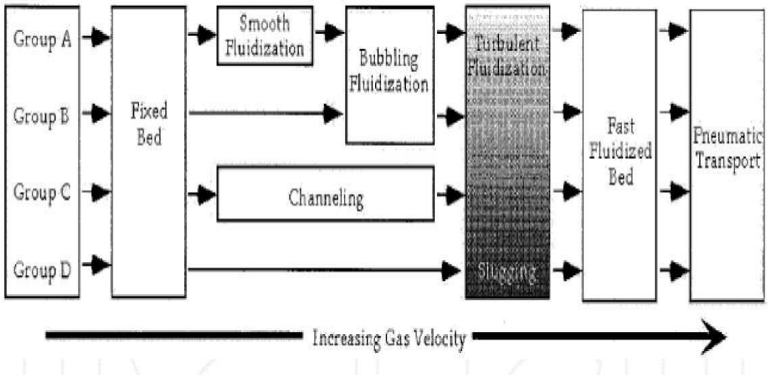

Figure 2.7: Powder behavior according to fluidisation regimes and Geldarts powder classification [10]

As seen, group A particles are well suited for fluidisation as it has smooth fluidisation phase between the fixed bed and bubbling regime. Group B is also fluidisable, however, this type of particles transcend directly to the bubbling regime from fixed bed. The final two groups, C and D go directly to a turbulent regime and are, therefore, not suited for fluidisation where transportation accuracy is of high importance.

2.3 Minimum Fluidisation Velocity

The minimum fluidisation velocity is defined as the velocity of the air in the transition point between the fixed- and bubbling bed regime and is one of the most important parameters for characterization of the fluidised bed. The minimum fluidising velocity V_{mf} is in most cases found experimentally. However, there are several formulas that can be used to estimate the velocity, one of which is the Ergun equation that will be described in this section.

The minimum fluidisation velocity is dependent on the properties of the solid material which in this case is the alumina properties. However, the minimum fluidisation velocity is also dependent on the bed geometry. D. C. Sau et al. (2007)[11] describes how a tapered bottom edge has effects on the fluidisation velocity. In this research they used different angles and found that an increase in the tapered angle also increases the minimum fluidisation velocity. Furthermore, N. Hilal et al. (2001) [12] found that increase in the bed diameter decreased the minimum fluidisation velocity in a cylindrical fluidisation column. This might be explained by the reduction the ratio between area affected by friction on the side walls to volume. This does, however, not have a significant influence on the transport accuracy and will, therefore, not be considered further.

2.3.1 Obtaining V_{mf} Experimentally

The minimum fluidisation velocity is as mentioned often found experimentally. The most common way of doing this is commonly known as the pressure drop method.

As previously explained in Figure 2.3 it is known that fluidisation occurs when

$$\text{(Drag force by gas)} = \text{(Weight of particles)}$$

that can be written as

$$\begin{pmatrix}\text{Pressure drop}\\ \text{across bed}\end{pmatrix}\begin{pmatrix}\text{Cross-sectional}\\ \text{area of slide}\end{pmatrix} = \text{(Bed volume)}\begin{pmatrix}\text{Fraction of}\\ \text{solids}\end{pmatrix}\text{(Specific weight)[6]}$$

With a positive pressure drop it can again be rearranged to Equation 2.1[6].

$$\frac{\Delta p}{L_{\mathrm{mf}}} = (1-\varepsilon_{\mathrm{mf}})(\rho_{\mathrm{s}}-\rho_{\mathrm{g}})g \tag{2.1}$$

This means that when a solid is fluidised the pressure drop over bed height is constant.

$$\frac{\Delta p}{L_{\mathrm{mf}}} = constant \tag{2.2}$$

The pressure drop is, therefore, measured by sensors in a fluidisation column where the superficial fluidisation velocity is gradually increased. When the bed reaches the criteria in Equation 2.2 a minimum fluidisation velocity is obtained as seen in figure 2.8.[13]

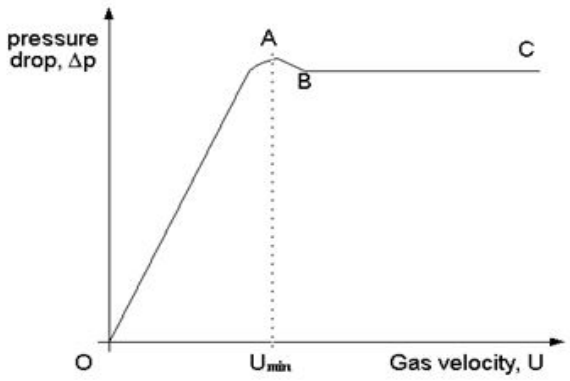

Figure 2.8: Typical pressure drop curve for increasing gas velocity [14]

2.3.2 Ergun Equation

The chemical engineer Sabri Ergun developed an equation that expresses the pressure drop correlation at the beginning of fluidisation based on drag force on single particles. Equation 2.3 shows this correlation with particles of the same size d_{p}, particle and fluidising medium density ρ_{s}, ρ_{g} and the fluidising medium viscosity μ_{g}. [6]

$$(1-\varepsilon_{\mathrm{mf}})(\rho_s-\rho_g)g = 150\frac{(1-\varepsilon_{\mathrm{mf}})^3}{\varepsilon_{\mathrm{mf}}^3}\frac{\mu_{\mathrm{g}}V_{\mathrm{mf}}}{(\phi_{\mathrm{s}}d_{\mathrm{p}})^2} + 1.75\frac{(1-\varepsilon_{\mathrm{mf}})}{\varepsilon_{\mathrm{mf}}^3}\frac{\rho_{\mathrm{g}}V_{\mathrm{mf}}^2}{\phi_{\mathrm{s}}d_p} \tag{2.3}$$

One of the challenges by using the Ergun pressure drop equation to estimate the minimum fluidising velocity V_{mf} is in addition to the assumption of all solid particles having the same size, the required knowledge of bed voidage $\varepsilon_{\mathrm{mf}}$ and the particle sphericity ϕ_{s}.

One common assumption is that voidage or porosity at minimum fluidisation velocity $\varepsilon_{\mathrm{mf}}$ approximately equals the porosity of the fixed bed. This is due to the minimum fluidising velocity being calculated at the point where drag force equals gravitational forces and the bed expansion will occur after this point. The porosity can then be calculated using Equation 2.4

$$\varepsilon_{\mathrm{mf}} \approx \varepsilon = 1 - \frac{\rho_{\mathrm{bnv}}}{\rho_{\mathrm{s}}} \tag{2.4}$$

The void fraction, also known as porosity shown in Equation 2.4 is a measurement of the empty space in the material and is, therefore, based on the relationship between the non vibrated bulk density and the particle density. The particle density could easily be defined and measured experimentally, however, the bulk density is not an intrinsic parameter. This means that the bulk density is subject to some variation based on the handling of the material. It is, therefore, important to note that ρ_{bnv} is measured in a normal, non-vibrated non-aerated state. The actual measurement is done by measuring weight and the volume occupied by the solid and determining density based on Equation 2.5.[10]

$$\rho_{\mathrm{bnv}} = \frac{M_{\mathrm{s}}}{V_{\mathrm{total}}} \tag{2.5}$$

Sphericity ϕ_s is on the other hand a calculation of the roundness of the particles. The sphericity is defined as the fraction of the area of a sphere with the same volume as the particle and the particle area as seen in Equation 2.6

$$\phi_s = \frac{A_{\text{sphere}}}{A_p} \tag{2.6}$$

The area A_{sphere} should, therefore, be expressed as a function of the particle volume as in Equation 2.7 that again can be found by the particle density and mass.

$$A_{\text{sphere}} = \pi^{\frac{1}{3}}(6V_p)^{\frac{2}{3}} \tag{2.7}$$

However, Wen and Yu [15] observed that the relationship between voidage and sphericity can be written as Equation 2.8 and 2.9 for spherical and non-spherical particles respectively. This is also shown in Figure 2.9 where ε_{mf} is plotted against ϕ_s.

$$\frac{1-\varepsilon_{\text{mf}}}{\phi_s^2\varepsilon_{\text{mf}}^3} = 11 \tag{2.8}$$

$$\frac{1}{\phi_s\varepsilon_{\text{mf}}^3} = 14 \tag{2.9}$$

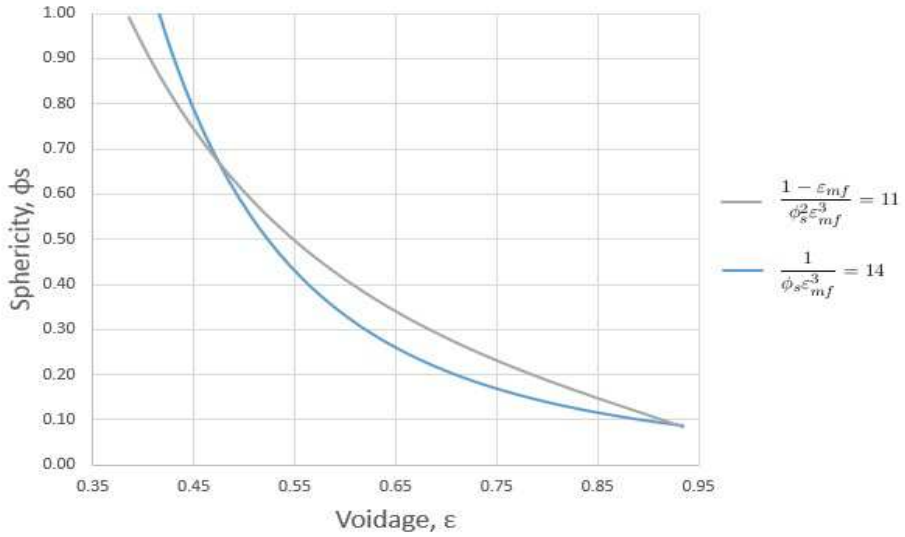

Figure 2.9: ε_{mf} plotted against ϕ_s based on Wen and Yu equations [15]

To calculate the minimum fluidisation velocity, V_{mf}, based on the Ergun pressure drop equation, a set of variables A, B and C is introduced to define Equation 2.3 as a an equation of second power.

$$C = AV_{\mathrm{mf}} + BV_{\mathrm{mf}}^2 \tag{2.10}$$

In Equation 2.10 A and B defines the viscous and inertial factor of the equation, while C is the weight per unit volume.

The minimum fluidising velocity could then be found by calculating the positive solution of the function of second power as in Equation 2.11.

$$V_{\mathrm{mf}} = \frac{-A + \sqrt{A^2 + 4BC}}{2B} \tag{2.11}$$

According to an article published by de Vasconcelos and Mesquita in cooperation with Albras Aluminio Brasiliero [16] it is also possible to simplify the equation even further. The low velocities related to fluidisation makes the factor B negligible. The minimum fluidising velocity could, therefore, be calculated by Equation 2.12 with an error of less than 5 % compared to Equation 2.11.

$$V_{\mathrm{mf}} = \frac{C}{A} = \frac{(\rho_{\mathrm{s}} - \rho_{\mathrm{g}}) g \varepsilon_{\mathrm{mf}}^3 (\phi_{\mathrm{s}} d_{\mathrm{p}})^2}{150(1 - \varepsilon_{\mathrm{mf}})\mu_{\mathrm{g}}} \tag{2.12}$$

2.4 Alumina Flow Modeling

The flow of alumina or the transport capacity of an air slide has been modeled by several researchers. In general the fluidised flow is commonly modeled as a open channel flow in Equation 2.13 where discharge is defined by the normal cross-sectional velocity, u and the wetted cross-sectional area, A [17]. What differentiates the different models is, however, the assumption of steady uniform flow or the use of a non-Newtonian model.

$$Q = \iint_A u dA \tag{2.13}$$

The steady uniform flow model has among others been used by K. Kennecke (1965) [18] and in previous work done by L. Haugland as cited by S. Valciu [19]. Steady open channel flow implies that the discharge of the slide is constant over time while uniform flow requires the bed height to be constant over the slide length [19]. Haugland did, however, conclude that flow of fluidised alumina was not steady and that non-Newtonian behaviour had to be investigated.

One commonly used model for non-Newtonian behaviour is the Saint Venant model as cited by R. Szymkiewicz (2010) [17] and C. E. Agu and B. Lie (2014) [20]. The governing one-dimensional Saint Venant equations 2.14 and 2.15 could, therefore, be used to model the unsteady open channel fluid flow.

$$\frac{\partial A}{\partial t} + \frac{\partial Q}{\partial x} = 0 \tag{2.14}$$

$$\frac{\partial Q}{\partial t} + \frac{\partial \left(\frac{\beta Q^2}{A}\right)}{\partial x} = gA\sin\theta - gA\cos\theta\frac{\partial h}{\partial x} - gAS_\mathrm{f} \tag{2.15}$$

The frictional slope S_f is given by Equation 2.16[20]

$$S_\mathrm{f} = \frac{\tau_\mathrm{y}}{\rho g h}\left(1 + \left(\frac{(\varepsilon+1)(\varepsilon+2)|V|}{(0.74+0.656\varepsilon)\left(\frac{\tau_\mathrm{y}}{K}\right)^{\varepsilon} R_\mathrm{h}}\right)^{\frac{1}{\varepsilon+0.15}}\right) \tag{2.16}$$

Table 2.1: Nomenclature for Saint Venant equations [21]

Q [m^3/s]	Volume flow rate
A [m^2]	Flow cross sectional area
h [m]	Alumina bed height
θ [degree]	Air slide inclination angle
g [m/s^2]	Gravitational acceleration
β	Momentum correction coefficient
R_h [m]	Hydraulic radius
τ_y [Pa]	Yield shear stress
$V = \frac{Q}{A}$ [m/s]	Average flow velocity
n	Degree of non-Newtonian behaviour of fluid
ρ [kg/m^3]	Alumina density
K [Pas^n]	Fluid consistency, larger K implies a more viscous fluid
ε	Roughness

2.4.1 Results from Previous Capacity Simulations

The Saint Venant equations 2.14 and 2.15 can according to S. C. Valciu et.al.(2014) [21] be reduced to Equation 2.17 for steady state alumina flow rate with a comparison of simulated and measured results in Figure 2.10.

$$Q = \frac{\cos(\theta)^{\frac{1}{2}} g^{\frac{1}{2}} b h^{\frac{3}{2}}}{\beta^{\frac{1}{2}}} \tag{2.17}$$

1,1 degrees							
	Operational parameters				Average capacity [t/hr]		
Pressure	U_0/U_{mf}	h_0 [m]	Q_0^{1000} [m^3/s]	Q_0^{950} [m^3/s]	Measured	Simulated$^{1000-950}$	Error$^{1000-950}$
3,0	0,99	0,126	0,00479	0,00504	17,9	17,2	3,7 %
3,5	1,16	0,119	0,00580	0,00611	20,9	20,9	-0,1 %
4,0	1,31	0,118	0,00611	0,00643	22,3	21,9	1,7 %
4,5	1,49	0,110	0,00658	0,00693	23,8	23,7	0,4 %
5,0	1,64	0,110	0,00695	0,00732	24,9	25,0	-0,2 %
5,5	1,81	0,102	0,00731	0,00769	26,1	26,3	-0,9 %
6,0	1,97	0,109	0,00747	0,00786	27,0	26,9	0,4 %
6,5	2,14	0,113	0,00785	0,00826	28,4	28,3	0,4 %

Figure 2.10: Comparison of measurements to the Saint Venant model (S. C. Valciu, 2014)[21]

Another interesting result from the report is that the air slide discharge rate seems to be more stable at lower pressures as seen in Figure 2.11. If this effect also is present on the point feeders it could mean that the dose accuracy could be increased by reducing the pressure.

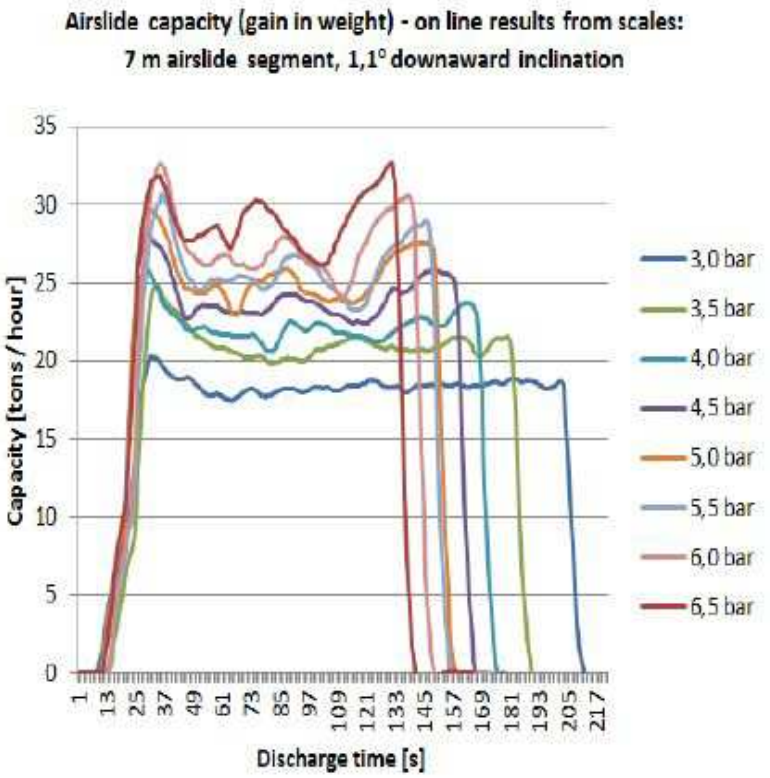

Figure 2.11: Measurements on air slide capacity (S. C. Valciu, 2014)[21]

2.5 Air Flow

The air flow is a very important parameter to the fluidisation of alumina. The air flow can be modeled using basic formulas from fluid dynamics and flow through nozzles. This section will, therefore, describe how the fluidising velocity is calculated based on pressure and system dimensions.

2.5.1 Converging-Diverging Nozzle

In the alumina air slide each aeration element is supplied by a main valve and equipped with converging diverging nozzles as seen in Figure 2.12 directly beneath the elements. The point feeders are on the other hand supplied by small pilot valves placed at a distance from the element together with a converging-diverging nozzle. This means that the air flow and the fluidising velocity can be calculated using formulas for flow in nozzles and the aeration element area.

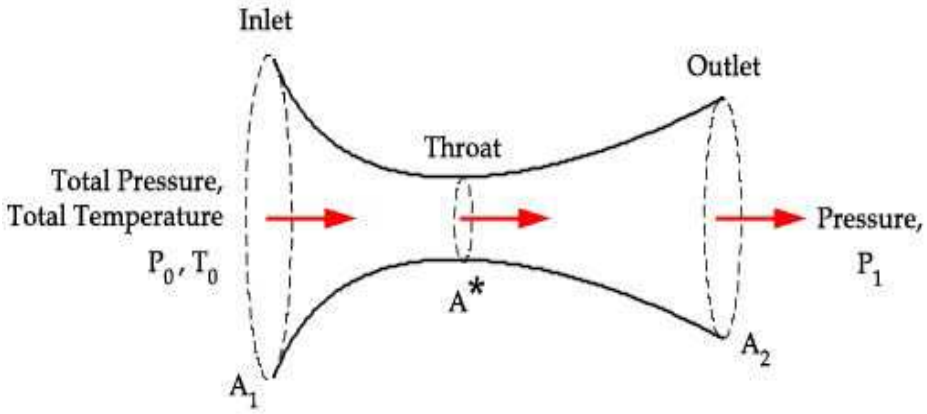

Figure 2.12: Illustration of the converging-diverging nozzle (source: ETBX)

The converging-diverging nozzle, also known as a De Laval nozzle is made up of a converging and diverging part as shown in Figure 2.12. The gas behavior in the nozzle depends on the back pressure, the air pressure at inlet and whether or not the gas reach sonic velocity in the nozzle.

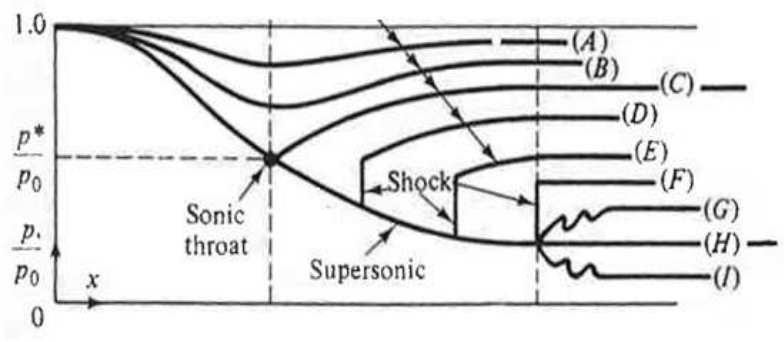

Figure 2.13: Illustration of gas behavior with back pressure to inlet pressure ratio plotted over nozzle length [22]

Figure 2.13 illustrates the gas behavior with reducing back pressure (A-I). It is then also possible to observe that the flow reaches supersonic velocity at the nozzle exit if $p_\mathrm{b} < p^*$. This relationship is important as the flow is chocked if the flow reaches a sonic velocity. Chocked flow means that the flow has reached a maximum and the only way to increase the mass flow is by increasing the nozzle diameter.[22]

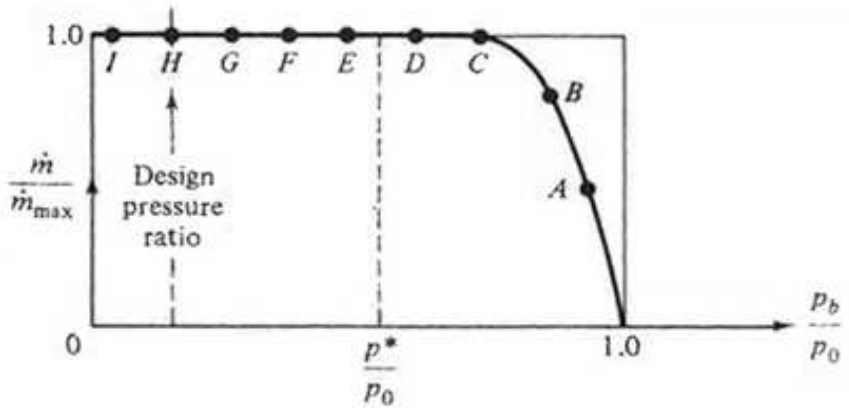

Figure 2.14: Graph showing mass flow ratio versus pressure ratio for nozzle flow [22]

In Figure 2.14 this phenomenon os also possible to observe where the mass flow ratio $\frac{\dot{m}}{\dot{m}_\mathrm{max}}$ is plotted against the back pressure ratio $\frac{p_\mathrm{b}}{p_0}$.

This means that if the critical condition $p_\mathrm{b} < p^*$ is reached, nozzle flow can be calculated from Equation 2.18. [22]

$$\dot{m} = \dot{m}_{\max} = \rho A V \tag{2.18}$$

The critical pressure is calculated from Equation 2.19

$$\frac{p^*}{p_0} = \left(\frac{2}{k+1}\right)^{\frac{k}{k-1}} \tag{2.19}$$

$$PV = nRT \tag{2.20}$$

With further simplification and introduction of the ideal gas law, Equation 2.20, the equation can be transformed to Equation 2.21

$$\dot{m} = \sqrt{\frac{k}{R_{\text{specific}}}} \frac{p_0}{\sqrt{T_0}} \left(\frac{2}{k+1}\right)^{\frac{k+1}{2(k-1)}} A_{\text{throat}} \tag{2.21}$$

Where R_{specific} is calculated from Equation 2.22 using the molar mass calculated in Table 2.2.

$$R_{\text{specific}} = \frac{R}{M} \tag{2.22}$$

Table 2.2: Properties of air (simplified)

Gas	Volume fraction	Molar mass, M [g/mol]	Specific heat ratio at 20° C and 1 atm, k
Oxygen	20.9	32	1.4
Nitrogen	79.1	28	1.4
Air	**100**	**28.84**	**1.4**

The remaining parameters used for calculation is presented in Table 2.3

Table 2.3: Parameters for calculation of air mass flow [22]

T_0 [K]	293
P_{b} [Pa]	1.5e05
ρ_{air} [kg/m^3]	1.2922
R [J/mol K]	8.314

Calculating the mass flow rate from Equation 2.21 the fluidising velocity could be calculated by the use of Equation 2.23.

$$V_0 = \frac{Q}{A_{\text{element}}} = \frac{\dot{m}\rho_{\text{air}}}{A_{\text{element}}} \tag{2.23}$$

2.5.2 Pressure Drop in Pipes

Calculation the fluidising velocity is as explained in the previous section done by using the inlet pressure of a nozzle in Equation 2.21. However, this calculation does not take pressure drop along pipe length due to frictional parameters into account. Another important factor is, therefore, the frictional losses in pipe flow. The nomenclature used for this calculation is presented in Table 2.4

Table 2.4: Nomenclature for calculation of pressure loss

Re	Reynolds number
$\overline{v}$	Average velocity
d	Pipe diameter
μ	Kinematic viscosity
f	Friction coefficient
g	Gravitational acceleration
ε	Pipe roughness
L	Pipe length
ρ	Density
h_f	Frictional head loss
Δp	Pressure drop
ζ	Resistance coefficient

To determine the pressure drop in pipes for air the first step is to calculate the Reynolds number using Equation 2.24 to determine whether the flow is laminar or turbulent.

$$Re = \frac{\overline{v}d}{\mu} \tag{2.24}$$

Depending on whether the flow is laminar ($Re < 2320$) or turbulent ($Re > 2320$) the friction coefficient can be calculated from Equation 2.25 and 2.26 respectively. [22]

$$f = \frac{64}{Re} \tag{2.25}$$

$$\frac{1}{\sqrt{f}} = -2.0 log_{10}\left(\frac{2.51}{Re\sqrt{f}} + \frac{0.269\varepsilon}{d}\right) \tag{2.26}$$

The solutions to the equations are also commonly plotted in a Moody diagram as shown in Figure 2.15.

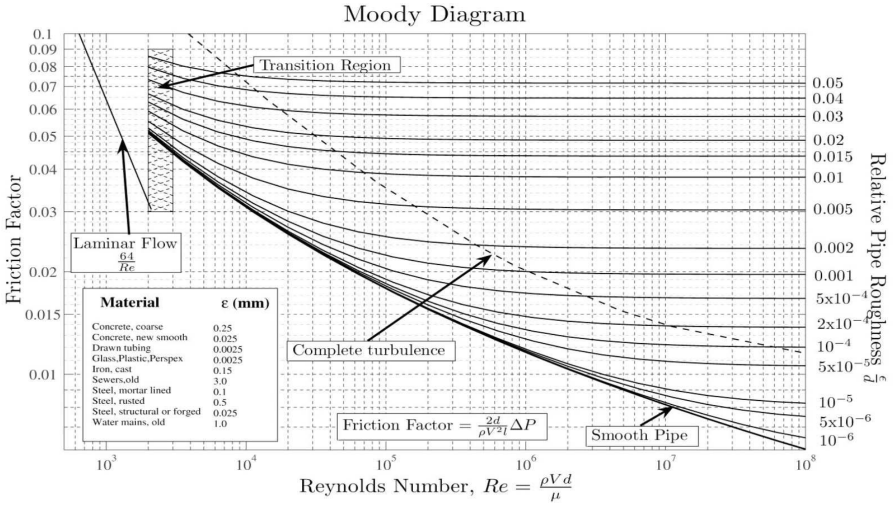

Figure 2.15: Moody diagram (source: Wikipedia)

The pressure drop for circular pipes could then be calculated by the use of Equation 2.27 and 2.28

$$h_{\mathrm{f}} = f\frac{L}{d}\frac{\overline{v}^2}{2g} \tag{2.27}$$

$$\Delta p = \rho g h_{\mathrm{f}} \tag{2.28}$$

Additionally it is necessary to include resistance in other elements such as valves, elbows, tees etc. The resistance coefficient for these elements is either provided by supplier or has to be found empirically. The loss from each of the elements are then found by Equation 2.29. [22]

$$\Delta p = \zeta\frac{\rho}{2}\overline{v}^2 \tag{2.29}$$

2.6 Alumina Properties

The smelter grade alumina or secondary alumina as it is called differs from the pure alumina in several properties and in this section an overview of the smelter grade alumina will be presented.

2.6.1 Chemical Purity

The chemical composition of secondary alumina is important when it comes to the physical properties. This is because the alumina has several impurities such as sodium oxide. This thesis will not address all the impurities and additions and rather look at the physical properties of the mixture that has an effect on fluidisation. It is, however, important to mention as the composition changes the physical behaviour of the alumina is also subject to variations.

2.6.2 Angle of Response

The angle of the response is an important factor when it comes to the aerated distribution system due to the level control which will be described at a later point in this report. The angle of response is defined as the constant angle of a cone pile of alumina. This angle is determined by the friction between grains and their ability to slide over each other. The basic physical properties that affect this is, therefore, the grain size and the grain distribution. Typical values of the angle of response is 30-36 degrees but can go as high as 40 for some types of alumina.

2.6.3 Density

For aerated distribution of alumina there are two important densities to address. This is first of all the real density. This is determined by the actual density of each separate grain and is often measured by the use of a displacing fluid in a pycnometer. For alumina the real density values are ranging from 3.45 to 3.60 kg/dm^3.

Bulk density is on the other hand not an intrinsic parameter as it can vary by the handling of the solid. The bulk density is defined as the mass of several particles divided by the total volume they occupy. This is, therefore, dependent not only on the particle volume, but also the inter-particle volume. Even though this is not an intrinsic parameter it is an important parameter for determining both the amount of alumina distributed to the cell and the fluidising velocity. The bulk density typically varies between 0.90 and 1.15 kg/dm^3.

Calculations in this thesis will be based on the values presented in Table 2.5.

Table 2.5: Density values used for calculation

Particle density [kg/dm^3]	3.500
Bulk density [kg/dm^3]	0.950

2.6.4 Particle Size Distribution

The particle size of the alumina is in addition to the density one of the most important factors for fluidisation. As most of the theoretical calculation is based on a uniform particle size, a

mean particle size has to be calculated based on the distribution. The distribution used will be presented, and a mean value calculated at a later point in this thesis.

Chapter 3

Evaluation of Current Design Variations

3.1 Minimum Fluidisation Velocity

Before evaluating the different designs it is very important to determine the fluidising velocity as this will be used as a dimensioning criteria for the system.

The results presented in this report is, therefore, based on tests of six different qualities by the use of a HELOS Particle size analysis performed by Sympatec and presented by K. Norheim (2013)[14]. Norheim divide the alumina into classes by the fraction of particles smaller than 45μm.

The classes M0-M4 are powder qualities referred to as fines. These can occur in production and cause changes to the alumina behaviour. In this report the results have primarily been included to validate the Ergun equation, E.q. 2.12. M5 is, however, representative for a normal alumina quality and further calculation will, therefore, be based on these results [14]. The different qualities are presented in Table 3.1.

Table 3.1: Alumina qualities used for testing

M0	**M1**	**M2**	**M3**	**M4**	**M5**
$10\% < 45\mu$m	$15\% < 45\mu$m	$20\% < 45\mu$m	$25\% < 45\mu$m	$30\% < 45\mu$m	$5\% < 45\mu$m

The report by K. Norheim [14] provide a thorough investigation of the particle size and cumulative distribution in the secondary aluminium. In Figure 3.1 the distribution of particles from the report is presented.

Using the information on actual particle size and weight fraction x_{i} provided by the Sympatec tests it is possible to estimate a mean value for alumina particle size d_{p} of the different qualities by the use of Equation 3.1. [16]

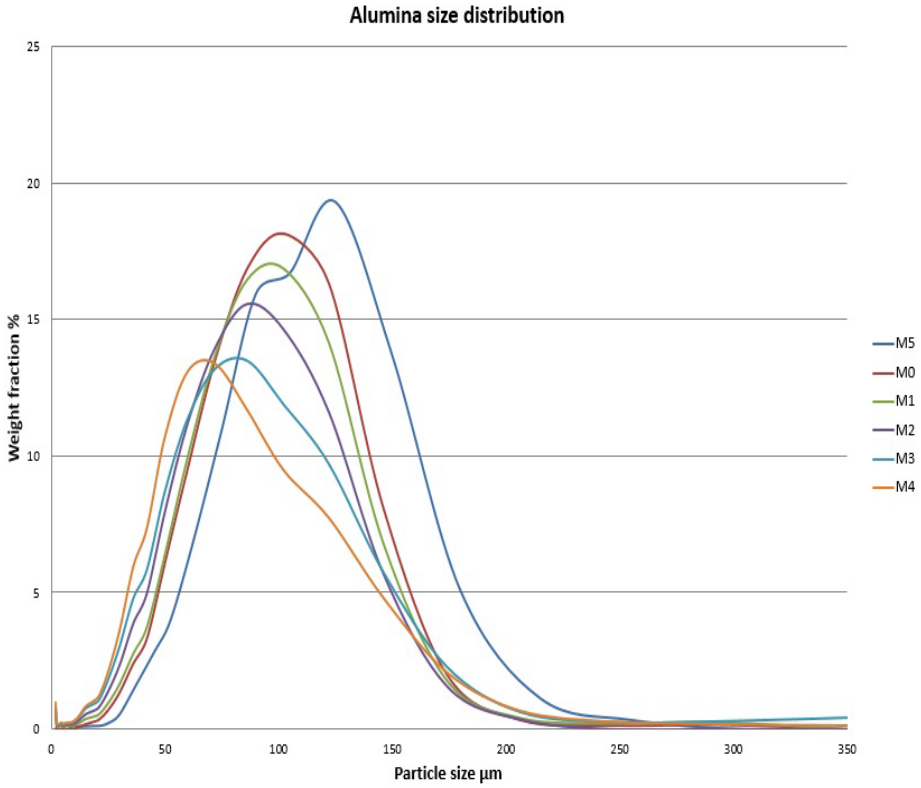

Figure 3.1: Distribution of particle size of alumina of five different qualities. M0, M1, M2, M3, M4 and M5. Data form K. Norheim [14]

$$d_{\mathrm{p}} = \sum d_{\mathrm{pi}} x_{\mathrm{i}} \tag{3.1}$$

This average particle size is used in the theoretical formulas to calculate the minimum fluidising velocity, V_{mf}. However, it is important to note that the formulas are based on the assumption that all particles are of the same size. Using an average particle size could, therefore, lead to errors.

The parameters used for calculation is presented in Table 3.2 and 3.3, including voidage calculated from Equation 2.4 and sphericity based on Figure 2.9.

Table 3.2: Properties of secondary alumina

Quality	M0	M1	M2	M3	M4	M5
$d_{\mathrm{p}}[\mu\mathrm{m}]$	91.18	86.73	80.05	79.39	73.26	105.87
$\rho_{\mathrm{s}}[\mathrm{kg/m^3}]$	3,500	3,500	3,500	3,500	3,500	3,500
$\rho_{\mathrm{b}}[\mathrm{kg/m^3}]$	950	950	950	950	950	950
ε	0.73	0.73	0.73	0.73	0.73	0.73
ϕ_{s}	0.19	0.19	0.19	0.19	0.19	0.19

Table 3.3: Properties of air and other constants used for calculation

$\rho_g[\mathrm{kg/m^3}]$	1.189
$\mu_g[\mu\mathrm{Pas}]$	18.602
$g[\mathrm{m/s^2}]$	9.82

By the use of the two tables and equation 2.12 explained in the previous chapter it is possible to estimate a minimum fluidising velocity V_{mf} theoretically. In Figure 3.2 the fluidising velocity is calculated according to the Ergun Equation 2.12 and compared to the experimental results from K. Norheim [14].

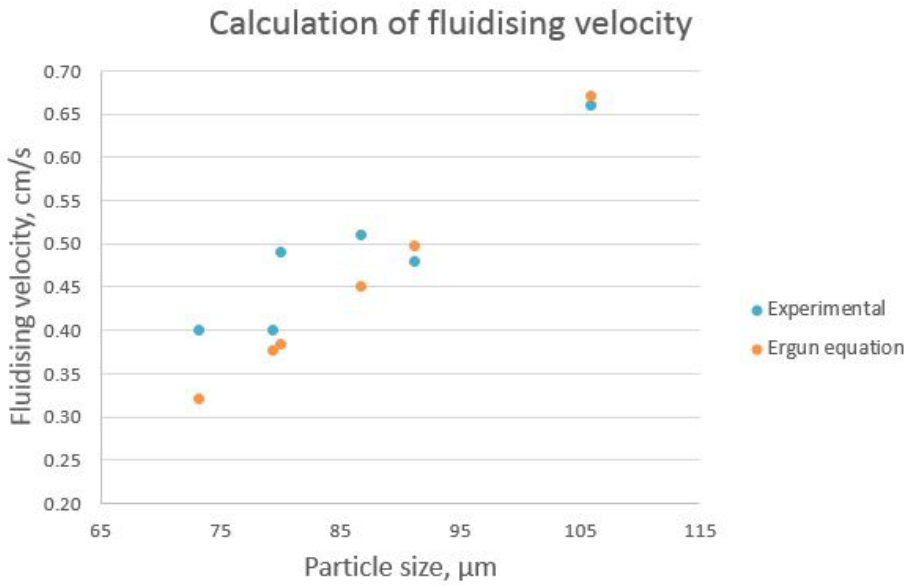

Figure 3.2: Theoretical calculation of fluidising velocity and experimental results

Observing the results presented in Figure 3.2 it is possible to see a clear correlation between the particle size and the minimum fluidising velocity. An increasing particle size results in a clear increase of the minimum fluidising velocity.

The experimental values were collected by the use of a fluidisation tester, measuring the pressure drop through the bed as explained earlier and used the same alumina qualities as used for the calculation. These results also show the same correlation between particle size and fluidising velocity, even though the calculated velocity is slightly higher. The experimental values are also shown separately in Figure 3.3.

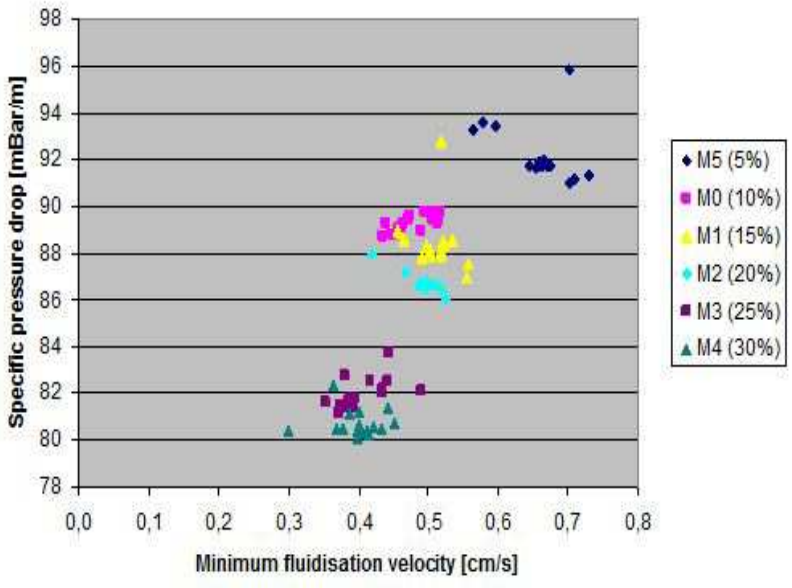

Figure 3.3: Results from experimental testing of minimum fluidisation velocity [14]

The report [14] concludes with a minimum fluidisation velocity of 0.66 cm/s while the Ergun equation gives 0.67 cm/s. Although, these values are close it is also shown in Figure 3.2 that the Ergun equation does not provide the same accuracy for all the tested qualities. In the rest of this report the experimental value of 0.66 cm/s will, therefore, be used.

3.2 Pressure Variations on Current Designs

The current designs in operation are dimensioned to operate with a fluidising velocity V_0 of 2.0 cm/s under optimal conditions. The high fluidising velocity is used to account for variation in the operational parameters such as supplied air pressure. The intention of this thesis is to investigate the efficiency and room for improvement for this system and it is, therefore, necessary to investigate this effect.

The pressure is a very important factor for the alumina distribution system. As explained earlier, the pressure is used to calculate required nozzles and supply pipes for the system. One of the main issues is, therefore, that the supplied pressure is not being kept at a constant level in the production.

Primarily, it is possible to divide the variations in the supply pressure into two different categories. One being internal effects, such as operation of the ADS on the cell (feeders and CAS) or the air consumption in the breakers. In other words are the internal effects defined as pressure variations caused by "on cell" standard operation.

The external effects are defined as "off cell" effects. This could be other standard or non-standard operations and effects from neighbouring cells such as cooling or other uses of the compressed air.

3.2.1 Internal Pressure Loss

As mentioned is the internal effects are caused by normal cell operation, such as operation of the alumina air-slide, point feeders and breakers. This could, therefore, be simulated using models for the cell and the standard operational parameters. The pressure loss due to these operations is easy to determine and they can be simulated with high accuracy.

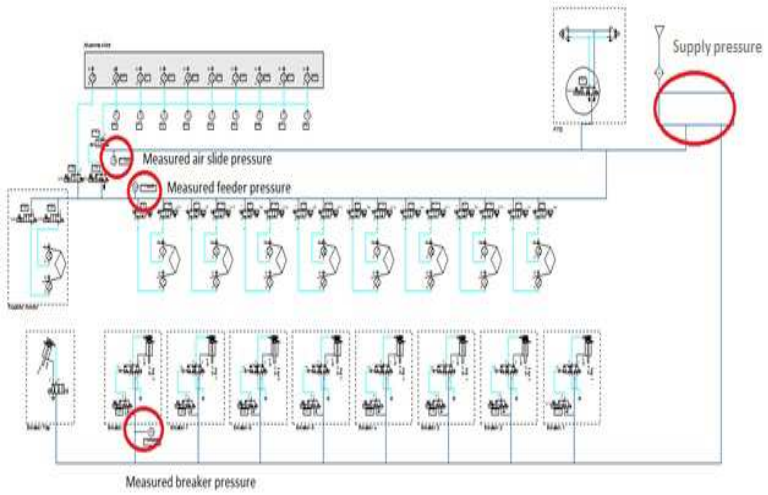

Figure 3.4: Illustration of the L22 model used to simulate pressure loss due to "on cell" operation

To simulate the pressure reduction FluidSim Pneumatics has been used for a L22 design shown in Figure 3.4. In these simulations, measurements have been carried out at the inlet for the supply valves. The results will have an insignificant variation on the different designs and are, therefore, representative for all the cells.

Figure 3.4 also illustrates where in the cell the measurements have been simulated to estimate the actual pressure exerted on various components. In reality the breakers could be considered as an "off cell" operation as they operate with a separate connection to the pressure grid, but are in this thesis considered as internal due to the placement in the cell.

The simulation has been carried out for a worst case scenario under normal conditions and 7.0 bar pressure on the net. This scenario is two feeder elements, the alumina air-slide and one breaker unit being operated simultaneously. P1 indicates the gauge pressure on the sensor with only the actual component running while P2 represents the worst case scenario. The results from these simulations are presented in Table 3.4. Due to a air save function in the breakers the air consumption reaches a maximum while the breaker is moving upwards. The value presented is, therefore, with the breaker moving upwards to its initial position.

Table 3.4: Table presenting simulated pressure loss on the components due to standard operation at 7.0 bar absolute pressure. P1 representing the operation of only the current component while P2 represents a worst case scenario with one breaker, two feeders and the CAS operating simultaneously

Component	P1 absolute pressure [bar]	P2 absolute pressure [bar]
Breaker (moving upwards)	6.93	6.50
Cell Air Slide	6.54	6.39
Point feeder (feeding element)	6.93	6.34

3.2.2 External Pressure Loss

The pressure fluctuations due to external effects are hard to determine by tests or simulations and requires observation over a long period of time to evaluate. This is due to the fact that the largest variations are caused by non-standard operations requiring a large consumption of compressed air.

The external loss could be caused by normal operation on neighbouring cells and bath tapping that occurs on a regular basis. It is also caused by much rarer events such as cooling of cells by the use of compressed air and other non-standard uses of the compressed air outlet.

Due to the difficulties related to the determination of this effect there is also a lack of documentation. The effect is, however, believed to result in pressure drops to as low as a 4.5 bar absolute pressure in extreme cases. For simulation purposes a pressure of 4.0 bar absolute pressure will be used to illustrate a worst case scenario taking into account both the internal and external pressure loss.

3.2.3 Pressure Measurements along Cell Air Slide

In addition to this, another important factor to address is to address is pressure loss along the cell air slide. An experiment carried out in 2014 by Serena Carmen Valciu [19] on a test rig in Porsgrunn indicate a significant pressure drop from first to last nozzle using a Ø10.7 mm inner diameter air supply.

No powder in the airslide							
Control box	3m	12 m				Total pressure loss	
1,4 mm nozzle	1,6 nozzle						
Pressure [bar]							
PT0	PT1	PT2	PT3	PT4	PT5	PT1-PT5	PT0-PT5
2,0	1,9	1,7	1,7	1,6	1,6	16 %	20 %
2,5	2,4	2,1	2,1	2,0	2,0	17 %	20 %
3,0	2,8	2,6	2,5	2,5	2,5	11 %	17 %
3,5	3,3	3,0	3,0	2,9	2,9	12 %	17 %
4,0	3,8	3,5	3,4	3,4	3,3	13 %	18 %
4,5	4,3	4,0	3,9	3,8	3,8	12 %	16 %
5,0	4,8	4,4	4,3	4,3	4,2	13 %	16 %
5,5	5,3	4,9	4,8	4,7	4,7	11 %	15 %
6,0	5,8	5,3	5,2	5,2	5,1	12 %	15 %
*1 x 1,6 nozzle, PT1 sensor on the 3 m airslide (not attached when testing with powder)							

Figure 3.5: Pressure loss measurement on CAS without powder in the slide [19]

Powder in the airslide							
Control box	3m	12 m				System pressure loss	
1.4 mm nozzle	1.6 mm nozzle						
Pressure [bar]							
PT0	*PT1	PT2	PT3	PT4	PT5	*PT1-PT5	PT0-PT5
2,0		Little or no powder transport					
2,5	2,4	2,1	2,0	2,0	2,0	18 %	20 %
3,0	2,7	2,5	2,5	2,4	2,4	12 %	20 %
3,5	3,2	2,9	2,9	2,8	2,8	16 %	20 %
4,0	3,7	3,4	3,3	3,3	3,2	14 %	20 %
4,5	4,0	3,7	3,7	3,6	3,6	15 %	20 %
5,0	4,7	4,3	4,2	4,2	4,1	16 %	18 %
5,5	5,1	4,7	4,6	4,6	4,5	14 %	18 %
6,0	5,7	5,2	5,1	5,0	5,0	15 %	17 %
*Estimated value, PT1 on the 3 m airslide (not attached when testing with powder)							

Figure 3.6: Pressure loss measurement on CAS with powder in the slide [19]

The tests were carried out using a pressure gauge mounted below each nozzle and the results from the slide without and with powder are shown in Figure 3.5 and 3.6 respectively.

These results also made it possible to validate the simulation software used. Comparing results from the test and the simulated values it is a clear correlation between the results as seen in Figure 3.7. The figure shows the correlation at 6.0 barg pressure and comparison with lower

pressure could be found in appendix A.1. The fact that the simulated results consistently show a lower pressure loss could be a result of small leakages in the actual system. Additionally it is also possible to observe that the alumina has little or no effect on the pressure loss in the cell air slide.

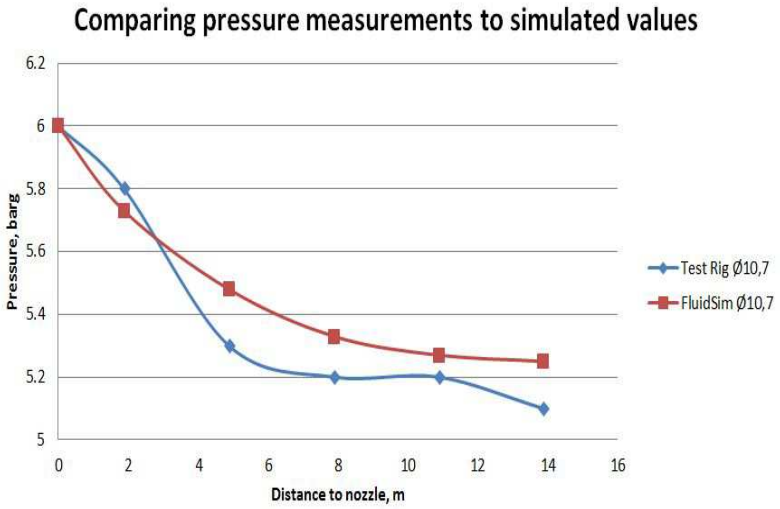

Figure 3.7: Comparison of simulated values using FluidSim and measurements from the Porsgrunn test rig at 6.0 barg

Due to the fact that the nozzles are dimensioned using nozzle Equation 2.21 from chapter 2 it is important that the pressure loss along the cell air slide is taken into account. This effect will be addressed for each cell design specifically in the next section.

3.3 Cell Air Slide

The cell air slide is used to supply alumina over the cell superstructure. Inside the cell air slide (CAS) there are ten aeration elements consisting of a nozzle and a porous fabric that forms the bed base. The Principle is that when the CAS is activated the alumina is fluidised allowing it to flow freely through the inclined channel.

Of the ten elements in the air slide only nine of them are used for the pneumatic conveying of alumina. The first element is on the other hand only used in short pulses to keep alumina from stagnating below the supply tube. This pillow operates at a higher fluidising velocity and with a separate air supply. It has, therefore, no focus for further calculations in this thesis.

Figure 3.8 illustrates the level control in the air slide and the reason for having an area beneath the inlet which is not fluidised. The principle is that the system utilises the alumina angle of response to set a steady state bed height. When the fluidisation elements are activated the alumina is fluidised but only above the elements. The steady state alumina level in the cell air slide is, therefore, determined by the angle of response for the solid alumina, the height from bed base to inlet pipe and the horizontal distance from the inlet to the first fluidisation element. The bed height can, therefore, be calculated by the use of simple trigonometry shown in Equation 3.2 and Figure 3.8.

$$h = H - d(tan(\alpha)) \tag{3.2}$$

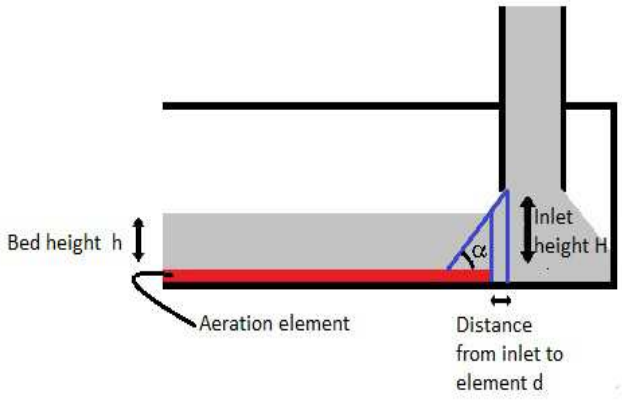

Figure 3.8: Illustration of level control in the cell air slide and parameters for calculation of bed height

The nine transportation elements are of high priority in this thesis due to the high fluidisation velocity of 2.0 cm/s. The different designs in current operation will, therefore, be investigated.

3.3.1 Air Supply Modifications

There are as mentioned currently six test cell in operation in the test center in Årdal with some variations in the cell air slide design (L22, L23, L24, L25, L26, L27). These variations are mainly on the nozzles below the aeration elements and piping for compressed air. This section will investigate the design variations to provide an overview of the current systems.

3.3.1.1 Design 1

The first design is based on the original NGC design parameters and is designed to maintain a fluidising velocity of $V = 2$ cm/s. This design is currently in operation on cell L22 and L23. The supply pipes for air is a Ø19 mm i.d. tube with connections to each of the nine aeration elements along the cell length. Table 3.5 presents the dimensions for nozzle diameter, element area and pipe length from the valve.

Table 3.5: Dimensions of the CAS aeration elements and nozzle diameter for the original NGC design

Element	1	2	3	4	5	6	7	8	9
Area[m^2]	0.1056	0.2510	0.1826	0.2852	0.2852	0.2852	0.2852	0.2852	0.3870
Nozzle[mm]	1.6	2.5	2.1	2.6	2.6	2.6	2.6	2.6	3.1
Distance[m]	3.0	4.3	6.0	7.7	9.9	12.0	14.2	16.3	18.6

A model for the cell was then created in FluidSim Pneumatics to simulate its functionality. The software allows measurements on pressure and volumetric air flow so that the fluidising velocity can be estimated. The parameters presented in Table 3.5 were, therefore, used to create the model presented in Figure 3.9.

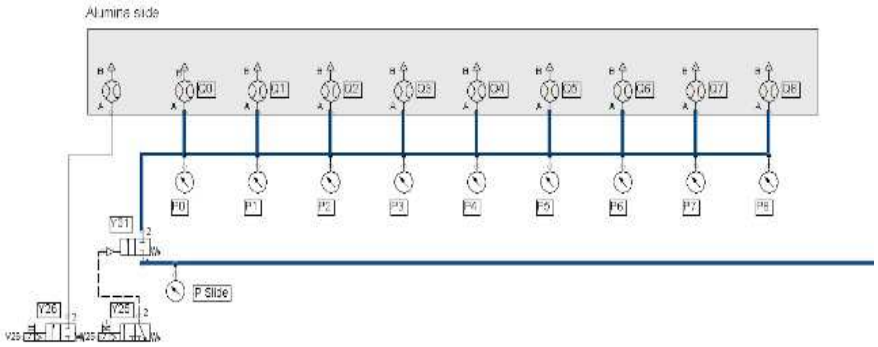

Figure 3.9: FluidSim model of design 1

As explained earlier the test rig in Porsgrunn discovered a high pressure loss over the cell length due to the diameter of the supply pipe. This effect was, therefore, investigated on the current

designs. The results from the pressure simulation over the cell length is shown in Figure 3.10 simulated for both high- (7.0 bar ABS) and low- (4.0 bar ABS) pressure from inlet.

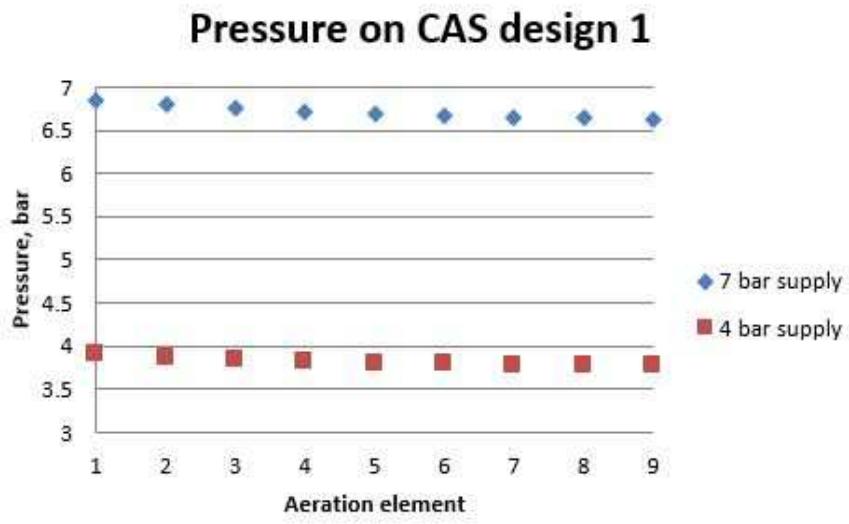

Figure 3.10: Pressure simulations for aeration elements on CAS design 1 showing a stable pressure over the cell length for 4.0 and 7.0 bar ABS pressure from inlet

As can be seen from these results the Ø19 mm pipe is large enough to maintain a stable pressure below each element. The nozzles are calculated and designed based on the absolute inlet pressure and it is, therefore, important that the pressure does not deviate significantly from the inlet pressure.

Due to this stable pressure it is also possible to observe that the fluidisation velocity is at a stable level for both high and low pressure as can be seen in Figure 3.11.

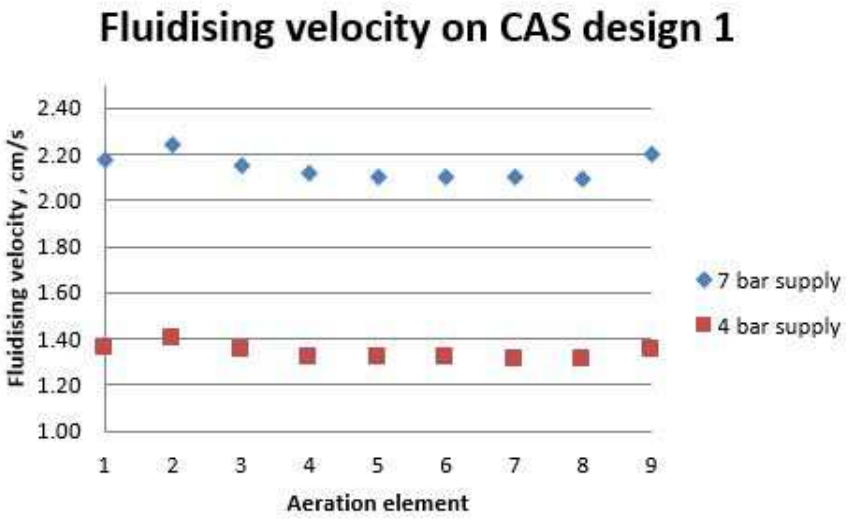

Figure 3.11: Simulations showing the fluidising velocity on the elements in CAS design 1 for 4.0 and 7.0 bar ABS pressure from inlet

The fluidising velocity is as can be seen, slightly higher than 2.0 cm/s and has improvement potential as the velocity can be reduced and thus reduce the air consumption. This will, however, be discussed further in the next chapter.

3.3.1.2 Design 2

The second design investigated uses a Ø12 mm air supply and nozzles as described in Table 3.6 and is the operating design on cell L24 and L25. In this design the pipe diameter has been reduced and the aeration elements has been equipped with a different set of nozzles. The reduction in pipe diameter was in addition to reduce the fitting and material costs and to reduce air consumption. However, as can be seen in Figure 3.12 this also increases the pressure loss due to the increased friction by reducing the volume to area ratio.

Table 3.6: Dimensions of the CAS aeration elements and nozzle diameter for the design used on cell L24 and L25

Element	1	2	3	4	5	6	7	8	9
Area[m^2]	0.1056	0.2510	0.1826	0.2852	0.2852	0.2852	0.2852	0.2852	0.3870
Nozzle[mm]	1.4	1.9	1.5	2.4	2.4	2.4	2.4	2.4	2.4
Distance[m]	3.0	4.3	6.0	7.7	9.9	12.0	14.2	16.3	18.6

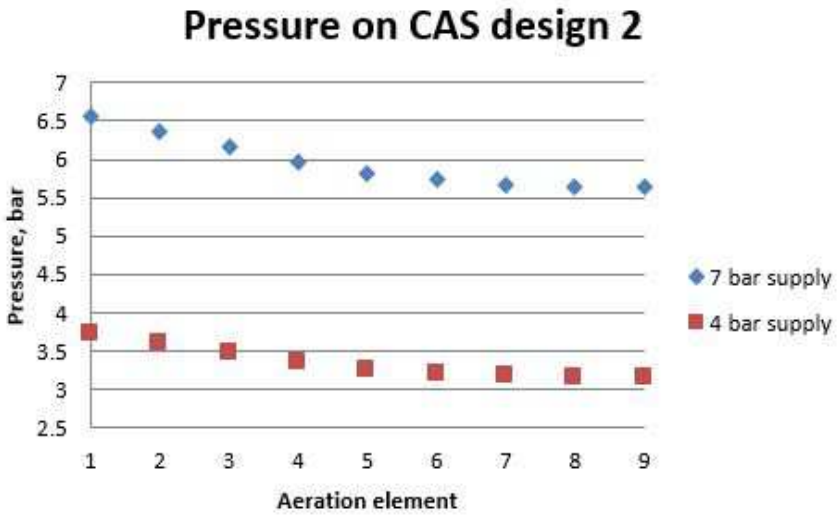

Figure 3.12: Pressure simulations for aeration elements on CAS design 2 showing a reduced pressure over the cell length for 4.0 and 7.0 bar ABS pressure from inlet

These results are closer to those for the alumina test rig in Porsgrunn equipped with a Ø10.7 mm air supply and a 19.5% pressure drop on the last element. What is seen here is also significantly higher than what should be considered an acceptable value. In addition to this pressure drop it is possible to detect an error in the nozzle design that causes a significantly lower fluidising velocity on the second, third and ninth transportation element.

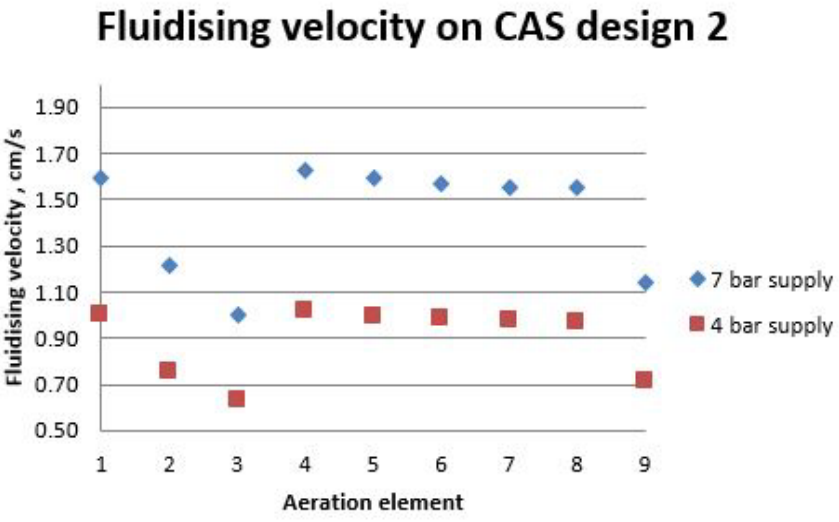

Figure 3.13: Simulations showing the fluidising velocity on the elements in CAS design 2 for 4.0 and 7.0 bar ABS pressure from inlet

Figure 3.13 shows the results from simulating the fluidising velocity on the second design.

Observing the graph for 4.0 bar pressure from inlet it is possible to see that the actual fluidising velocity is close to what is expected to be minimum fluidising velocity $V_{mf} = 0.66$cm/s based on empirical testing described earlier.

In this design the second, third and ninth element will also be considered weak links and the safety factor on the other elements becomes unnecessary. This is due to the fact that if one of the elements in the cell air slide fails to transport alumina because of a too low fluidising velocity or other conditions, the whole slide will lose its functionality. The high fluidising velocity on the other elements has, therefore, no beneficial contribution to the process and only results in a higher consumption of compressed air.

3.3.1.3 Design 3

The third design investigated is also close to the original NGC design as seen in Table 3.7. Compared to design 1 the only difference is a reduction in the pipe diameter for compressed air supply. However, the supply pipe is larger than the one used for design 2 with an inner diameter of 15 mm.

Table 3.7: Dimensions of the CAS aeration elements and nozzle diameter for the L26 and L27 design

Element	1	2	3	4	5	6	7	8	9
Area[m^2]	0.1056	0.2510	0.1826	0.2852	0.2852	0.2852	0.2852	0.2852	0.3870
Nozzle[mm]	1.6	2.5	2.1	2.6	2.6	2.6	2.6	2.6	3.1
Distance[m]	3.0	4.3	6.0	7.7	9.9	12.0	14.2	16.3	18.6

As seen in Figure 3.14 the reduction to a Ø15 mm pipe in an improvement from the second design. Even though there are possible to see a slight reduction in the pressure from first to last element, the design comes close to the pressure stability offered by the first design.

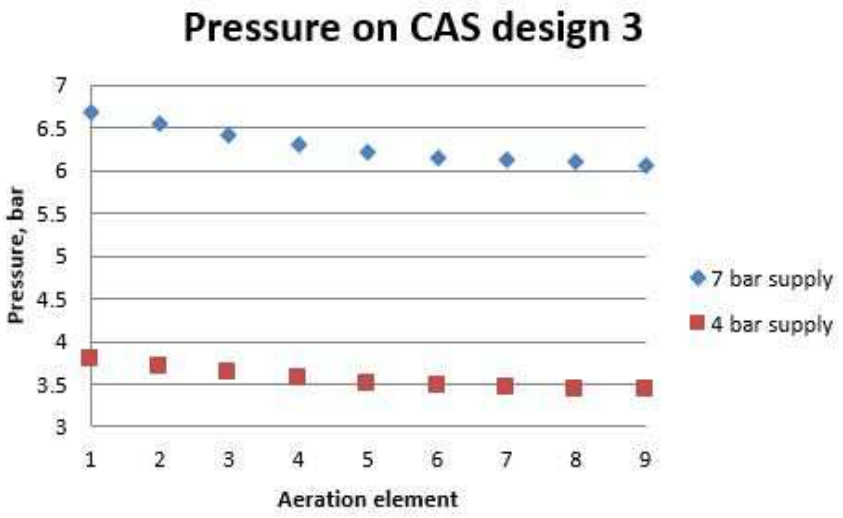

Figure 3.14: Pressure simulations for aeration elements on CAS design 3 showing a reduced pressure over the cell length for 4.0 and 7.0 bar ABS pressure from inlet

Seeing as this design is made up of the same nozzles found in the first design the fluidising velocity is expected to show the same trend over the nine elements with an increasing reduction towards the last elements due to the pressure loss.

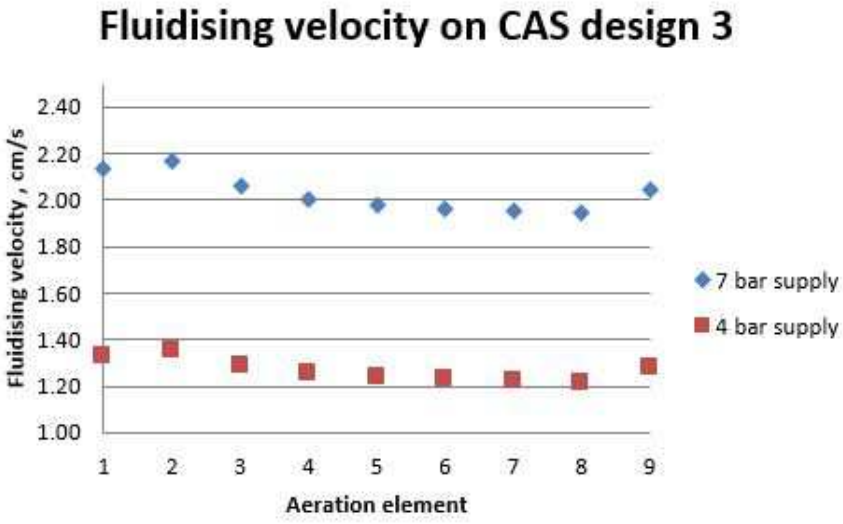

Figure 3.15: Simulations showing the fluidising velocity on the elements in CAS design 3 for 4.0 and 7.0 bar ABS pressure from inlet

The results from the simulations in Figure 3.15 does as expected show a slight reduction in fluidising velocity from the first design. The fluidising velocity is, however, still kept at a relatively stable level without certain elements limiting the functionality as in design 2.

3.3.2 Design Comparison

The most important criterion for the cell air slide design is the ability to deliver alumina to the feeders and thus to provide a fluidisation velocity high enough to maintain a sufficient capacity. The fact that the alumina supply is crucial for the aluminium production also makes it necessary with a margin of safety to account for abnormal conditions in the current design.

Table 3.8: Comparison of fluidising velocity V[cm/s] on the aeration elements in design 1, 2 and 3 with 7.0 bar absolute pressure

Element	Design 1	Design 2	Design 3
1	2.18	1.59	2.13
2	2.24	1.22	2.17
3	2.15	1.00	2.06
4	2.12	1.62	2.00
5	2.10	1.59	1.98
6	2.10	1.57	1.96
7	2.10	1.55	1.95
8	2.09	1.55	1.95
9	2.20	1.14	2.05
Avr	2.14	1.43	2.03
Min	2.09	1.00	1.95
STDEV	0.05	**0.22**	0.08

Based on the results from the simulations of the current designs, all three are within a functional area during normal conditions and a 7.0 bar absolute pressure from the pressure grid as can be seen in Table 3.8. It is, however, important to note that the element to element variation on design 2 is high compared to the other two. This is as mentioned caused by the under-dimensioned nozzles on the second third and ninth element. Comparing design 1 and 3 does, however, show the effect of the pressure loss over the cell length on the fluidising velocity. This factor is the one and only reason for the increased standard deviation on design 3 compared to design 1.

Table 3.9: Comparison of fluidising velocity V[cm/s] on the aeration elements in design 1, 2 and 3 with 4.0 bar absolute pressure

Element	Design 1	Design 2	Design 3
1	1.36	1.00	1.33
2	1.40	0.76	1.35
3	1.35	0.63	1.29
4	1.32	1.02	1.25
5	1.32	0.99	1.24
6	1.32	0.98	1.23
7	1.31	0.98	1.22
8	1.31	0.97	1.22
9	1.35	0.71	1.28
Avr	1.34	0.89	1.27
Min	1.31	**0.63**	1.22
STDEV	0.03	**0.14**	0.05

The results in Table 3.8 does indicate that design 2 might not be able to maintain a fluidising velocity higher than the minimum requirement V_{mf} under a 4.0 bar pressure. The fact that this is a simulation of worst case conditions does not necessary mean it would fail. It is, however, considered to be the least favorable design based on these results.

Next it is important to address the air consumption in the cell air slide. Seeing as design 3 maintains a slightly lover average value for fluidisation velocity, it also has the lowest air consumption of the two remaining designs. It is, therefore, preferable to the original NGC design as is today. This is mainly due to the fact that the alumina transport capacity is higher than necessary with a run time of 30 sec on the cell air slide, even with a fluidisation velocity of $V_0 = V_{\text{mf}}$ [19]. This will, however, be explained thoroughly in the next chapter.

On the other hand the results indicate that the original NGC design (design 1) has the highest potential for improvements such as pressure reduction or re-dimensioning of nozzles. This is due to the fact that the dimensioning element will be the one with the lowest fluidising velocity and that design 1 has a lower standard deviation on fluidising velocity from element to element compared to design 2.

Table 3.10: Comparison of air consumption on design 1, design 3 and modifications on design 1 with reduced pressure and new nozzles according to Table 3.11

Design	Air consumption [m^3/s]	Reduction compared to NGC
Design 1 (NGC)	0.0504	N/A
Design 3	0.0475	5.7%
NGC with 5.5 bar	0.0409	18.78%
NGC new nozzles	0.0420	16.70%

In Table 3.10 the total air consumption for design 1 and design 3 is shown. Design 3 is here left out due to the fact that it is not considered reliable based on the first criterion for the

fluidised air slide. The table also includes a proposition for improvement on the cell air slide with two possible options for reduction on air consumption both dimensioned after a superficial fluidising velocity $V_0 = 1.7$cm/s criterion.

The first option is a reduction to 5.5 bar using a dynamic pressure regulator. A value for the volumetric flow (Q) was calculated based on a fluidising velocity of 1.7 cm/s and the element area by formula 3.3.

$$Q = VA \tag{3.3}$$

This value was later used as a minimum requirement in the simulation software where the pressure was gradually reduced. The lowest possible pressure maintaining the minimum requirement for volumetric flow was, therefore, estimated to 5.5 bar absolute pressure. The new fluidising velocities is shown for each element in Figure 3.16.

The other alternative is a redesign of the nozzles using the equations for nozzle flow explained earlier. The new nozzles, dimensioned for a fluidising velocity of 1.7 cm/s at a 7.0 bar absolute pressure in Table 3.11 was then applied to the FluidSim model. In this case the fluidising velocity of 1.7 cm/s was used as a minimum criterion and the nozzle diameter was calculated to the closest 0.1 mm above this value. This is mainly due to the production cost when introducing lower tolerances. A closer value is, therefore, theoretically possible but not considered due to the high costs. The values for fluidising velocity on each element with the new nozzles is also shown in Figure 3.16.

Table 3.11: New nozzle dimensions for Design 1 using $V = 1.7$cm/s as a dimensioning criterion

Element	1	2	3	4	5	6	7	8	9
Nozzle[mm]	1.5	2.2	1.9	2.4	2.4	2.4	2.4	2.4	2.7

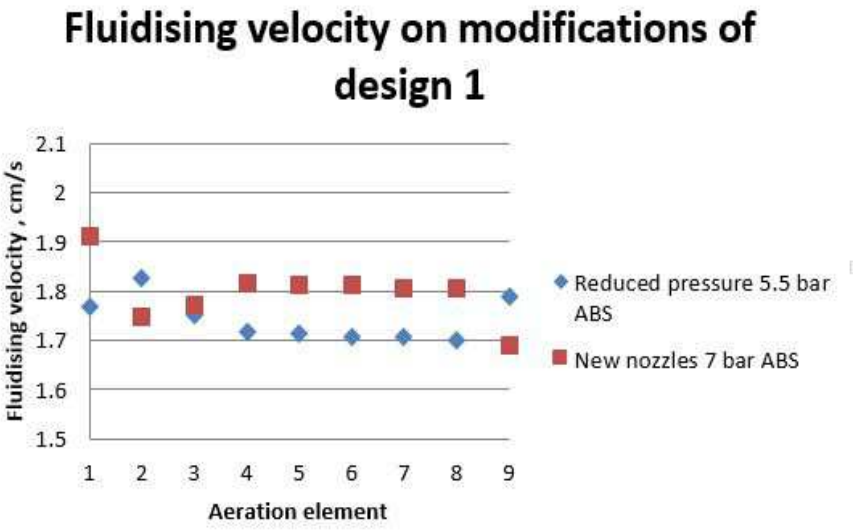

Figure 3.16: Fluidising velocity on each aeration element with pressure regulator to 5.5 bar or reduced nozzle diameters according to Table 3.11

Both of these options could theoretically result in a 15-20% reduction in air consumption even though the use of a dynamic pressure regulator has a couple of advantages. First of all does the use of a pressure regulator maintain the same margin of safety as the original design for pressure dropping below the set value of 5.5 bar. This does, however, require the dynamic regulator to have a functional area ranging between at least 5.5 to 7.0 bar absolute pressure. The option with modified nozzles will, however, have a reduced fluidising velocity of close to 1.0 cm/s as can be seen in Figure 3.17.

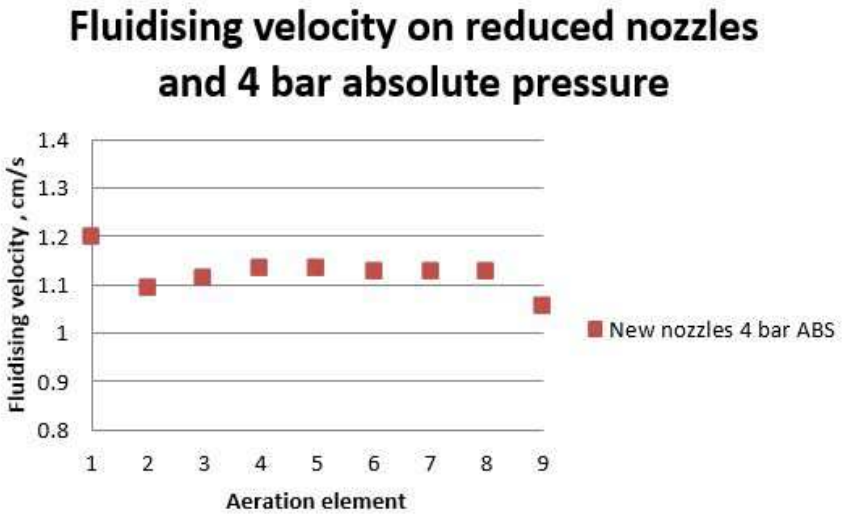

Figure 3.17: Fluidising velocity on each aeration element for reduced nozzle diameters from Table 3.11 and a 4.0 bar pressure

Secondly, the use of a pressure regulator leaves room for a further reduction of fluidising velocity without major operations and the ability to adjust back if other factors should result in a need for higher fluidising velocity e.g. change in the alumina quality. The downside is, however, the equipment cost and a possible increase in maintenance.

3.4 Point Feeders

There are currently six HAL4e cells operating with some variation in the point feeders in Årdal. However, they all operate by the same principle with a control volume, aeration elements for filling and emptying.

In the point-feeders both upper and lower element (to and from control volume) are supplied by a pilot valve each. In most cases these have been placed in a pneumatic cabinet next to the cell due to accessibility. There are, however, cells where the pilots are located in direct proximity of the feeder unit.

3.4.1 Design Variations

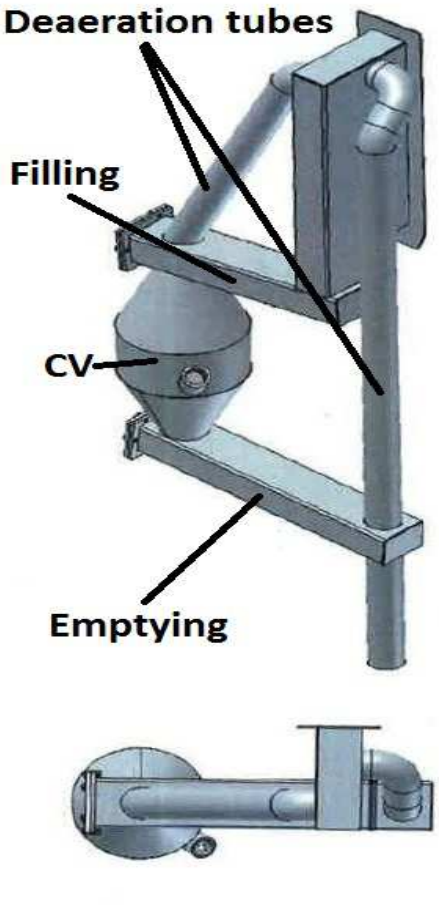

Figure 3.18: Model of the L23 point feeder

The point feeder at L23 is shown in Figure 3.18 with the control volume, feeding- and filling element visible. The figure also presents the general overview of all the feeders as the main variations are the parameters for deaeration tube, control volume and element lengths. The actual design variations for the point feeders are not presented due to confidentiality, but the main differences will be described where necessary.

3.4.2 Previous Measurements on Current Designs

The feeder data collected from measurements between 2011 and 2014 conducted by H. Kueppers [23] provides some input to the current designs. The raw data has been investigated and Table 3.12 present a general overview of the results.

Table 3.12: Feeder data overview [23]

Cell	L22	L23	L24	L25	L26	L27
Date tested	27.11.13	09.12.14	24.08.11	10.07.13	N/A	06.09.12
Average CV [g]	18,376	20,475	12,608	12,383	13,412	14,133
STDEV CV [g]	362	213	420	72	399	279
RSD CV	2.0 %	1.0 %	3.3 %	0.6 %	3.0 %	2.0 %
CVs emptied	20	22	30	30	15	30
Doses taken	160	1056	240	240	120	240
Average dose [g]	919	931	420	413	894	471
STDEV dose [g]	176	159	68	48	289	73
RSD dose	19.2 %	17.1 %	16.2 %	11.6 %	32.3 %	15.5 %

The main difference on the designs presented in Table 3.12 is that the de-aeration tube has a smaller diameter on the L26 design. This could be the reason L26 operates with a higher relative standard deviation on doses.

In theory, an insufficient venting could lead to excess air being vented out through the feeding element rather than the de-aeration tube. This air will carry alumina out through the feeder and might, therefore, be the reason for the significant increase in RSD for feeder L26. Other than this, no other design variations show a consistent change in dose accuracy.

Another factor affecting the standard deviation in the doses is the standard deviation in the control volume. As explained previously, the control volumes are being emptied each cycle to improve the feed control and make sure a sufficient amount of alumina is supplied to the cell. This means that a deviation in the control volume will have a large effect on the last doses which is represented with cell L24 in Figure 3.19 where the last dose varies between being too large and too small. The fact that the control volume and feeding slide is emptied can also effect the first dose as the conditions are different from what can be considered a steady state feeding which in this case is between dose 2 and 26.

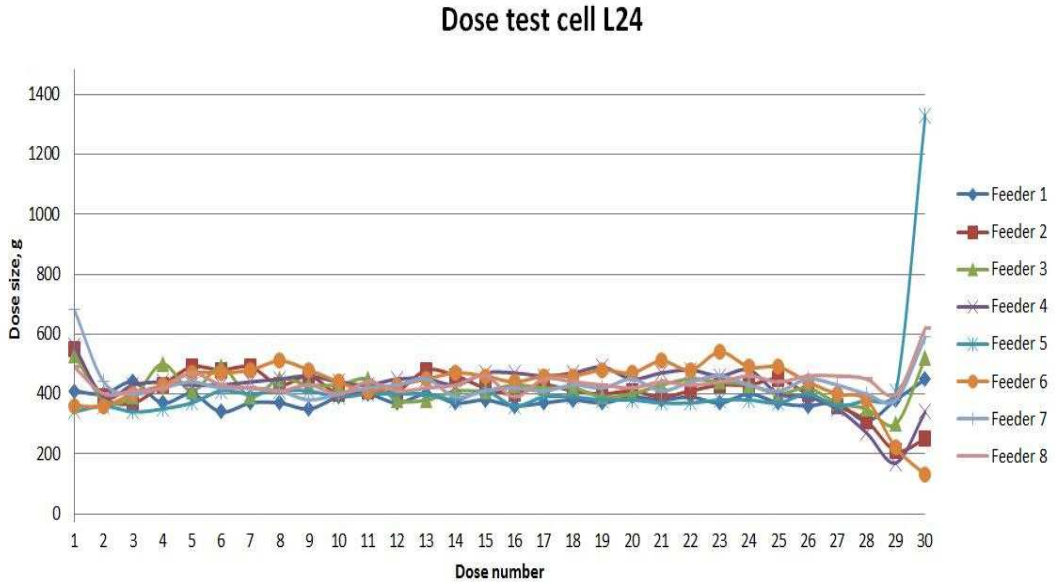

Figure 3.19: Doses measured on cell L24 showing the startup and end effects caused by emptying the control volume each cycle

Compared to the doses from L26 presented in Figure 3.20, cell L24 actually show a high stability when considering the doses without the startup and end effects for each cycle. Another calculation of the standard deviation in dose size was, therefore, carried out only including the area unaffected by the startup and end cycle and is presented in Table 3.13.

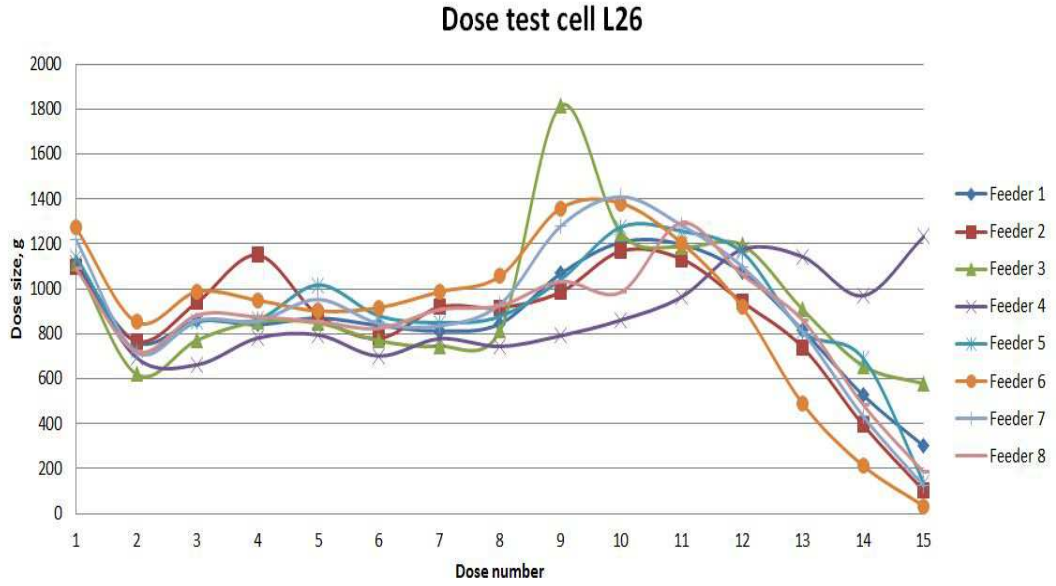

Figure 3.20: Doses measured on cell L26 showing an unstable dose size over the entire cycle

Table 3.13: Feeder data considering doses without startup and end cycle effects

Cell	L22	L23	L24	L25	L26	L27
Average dose [g]	927	904	418	421	949	488
STDEV dose [g]	83	69	29	35	163	43
RSD dose	9.0 %	7.7 %	7.0 %	8.3 %	17.2 %	8.9 %

In Table 3.13 where the standard deviation has been calculated without consideration of the first and two last doses it is still possible to observe that the relative standard deviation on cell L26 is significantly higher then what is observed on the other cells. Based on the observations made in Figure 3.20 this is expected but it provides credibility to the assumption that the de-aeration tube is under dimensioned. This is due to the fact that this is the only major design variation when the effect of control volume deviation has been eliminated.

The remaining cells show a relatively similar RSD which indicate that the variation in designed control volume (18 kg/12 kg) does not have a significant effect.

3.4.3 Fluidising Velocity and Valve Placement

To inspect the feeders FluidSim was used to create a cell model. The model shown in Figure 3.21 was used to simulate the flow on the first and last (eight) feeder. The remaining elements will have a behaviour in between the two extremes and are left out of the discussion.

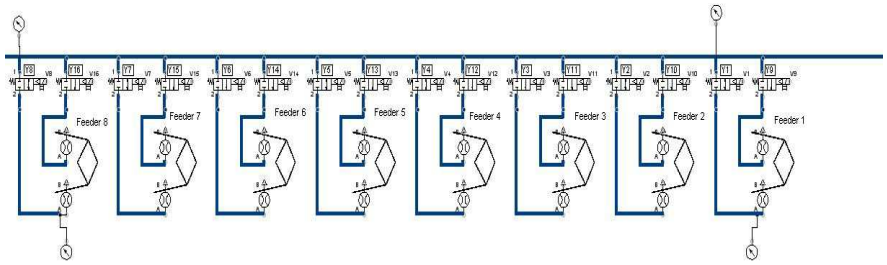

Figure 3.21: Illustration of the FluidSim simulation model for the feeders

Simulation and testing of the feeder system shows a major over dimensioning of the nozzles connected to the feeder aeration elements. As a result there is a fluidising velocity reaching 8.0 cm/s on the feeding units based on simulations done in FluidSim seen in Figure 3.22. The feeding units are equipped with a Ø1.2 mm nozzle and with a 7.0 bar absolute pressure for all the different point feeder designs. The main reason the point feeders operate with these parameters is the cost of producing nozzles smaller than 1.2 mm and that this cost exceeds the possible savings with respect to the air consumption.

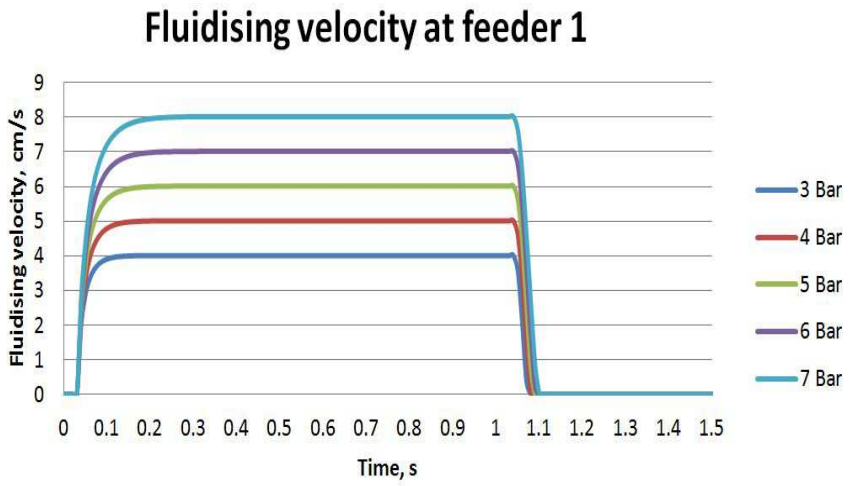

Figure 3.22: Fluidising velocity on feeding element on feeder 1 with valve placed 6.5m from the element and pressure from 3.0-7.0 bar absolute pressure

Taking cell L22 as an example, the eight feeders are required to supply a total of 7046 900 gram doses per day which with a time period of 3.5 seconds per dose results in a consumption of about 9,000 normal cubic meters of compressed air per year per cell. A quick estimation using a cost of 0.08 NOK/m^3 results in a cost of 720 NOK/cell/year and a 50 % reduction in air does not have a significant effect. The cost of new nozzles can, therefore, not be justified based solely on reduced air consumption. This does not only apply for nozzles but the implementation of a pressure regulator also has to show other results to be justifiable.

However, from the results of the simulations with a one second pulse on the feeding element with varying pressure shown in figure 3.22 it is possible to observe that there is an increase in the time the element operates with a steady state fluidising velocity with lower pressure. Observing this more closely in Figure 3.23 it is shown that the transient phase could be reduced with about 0.08 seconds by reducing the pressure from 7.0 to 3.0 bar absolute pressure.

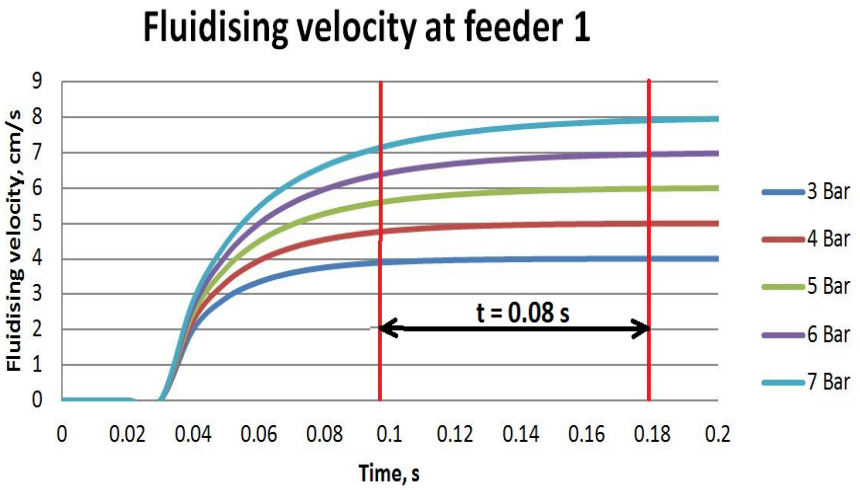

Figure 3.23: Figure showing the time reduction of a transient phase by reduction of pressure

This effect is even more visible when it comes to feeder 8 the transient phase is longer due to the time it takes to build up pressure in the pipe leading from the valve placed in the pneumatic cabinet to the aeration element inside the cell. On the first feeder this distance is estimated to 6.5 meters while the distance to feeder number eight is estimated to 19 meters. The results for simulations on feeder eight is shown in Figure 3.24.

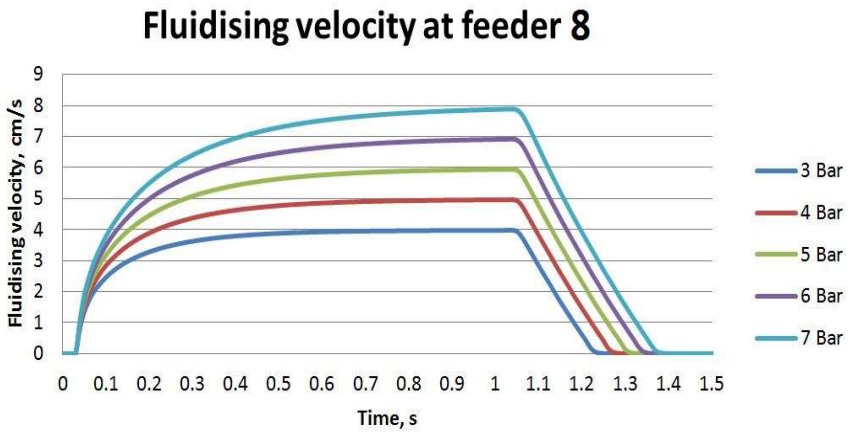

Figure 3.24: Fluidising velocity on feeding element on feeder 8 with valve placed 19m from the element and pressure from 3.0 - 7.0 bar absolute pressure

On the filling element of the feeder the same effect is observed but in this case the elements are operating on a much lower fluidising velocity as the aeration element in the filling slide has a significantly larger area. In this case the fluidising velocity is closer to the critical level when

pressure is reduced as seen on the first feeder in Figure 3.25

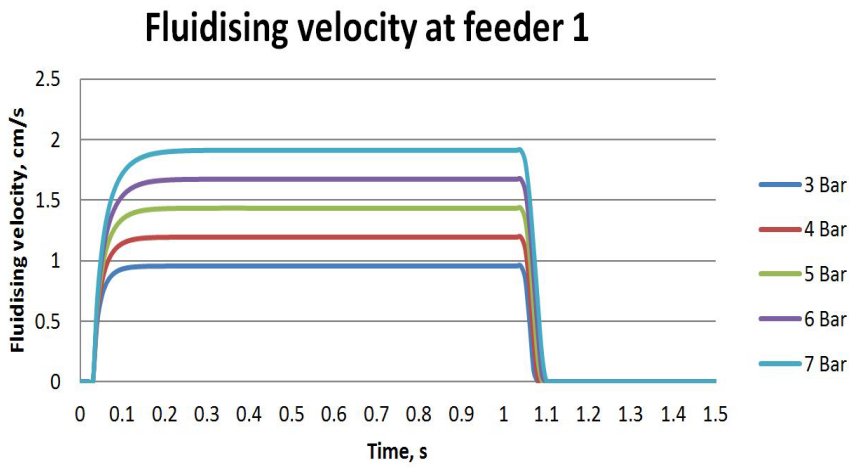

Figure 3.25: Fluidising velocity on filling element on feeder 1 with valve placed 6.5 m from the element and pressure from 3.0-7.0 bar absolute pressure

A closer look shows that small delay from where the filling element reaches minimum fluidisation velocity $V_{\text{mf}} = 0.66$ cm/s on feeder one as seen in Figure 3.26. Whereas the transition phase has a hypothetical effect on the alumina feeding as the capacity follows a power curve, a time delay from where the powder reaches fluidising velocity can have a large effect as the powder will remain in a solid state.

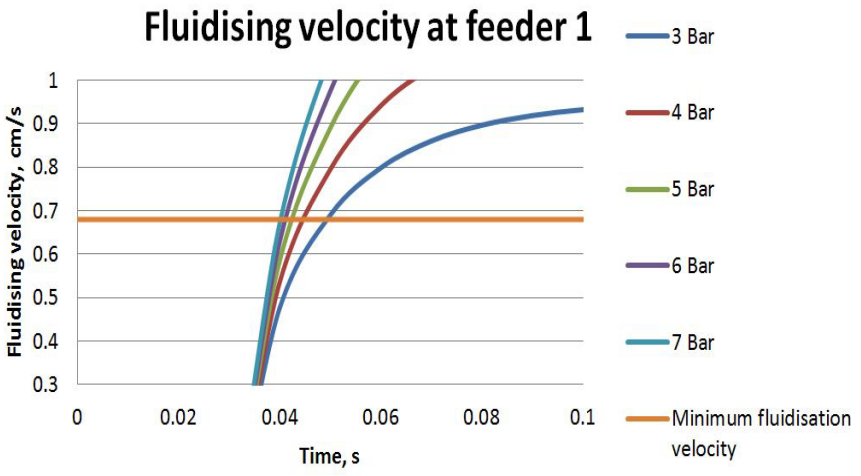

Figure 3.26: Graph showing a present time delay from 7.0 to 3.0 bar absolute pressure for where the filling element on feeder 1 reaches minimum fluidisation velocity

Even though the effect is small on feeder one, feeder eight is more critical, as seen in Figure 3.27. On the eight feeder this delay can be as large as 0.07 seconds from 3.0 to 7.0 bar

absolute pressure. It is, however, possible to correct for this effect by running the elements with individual parameters for fluidisation time. In other words, having individual control of each feeder based on the distance from the pneumatic cabinet is considered to be necessary.

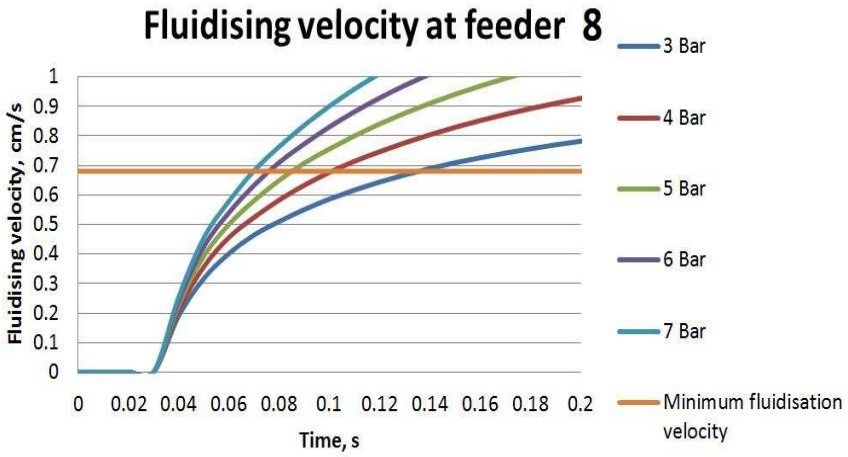

Figure 3.27: Graph showing a significant time delay from 7.0 to 3.0 bar absolute pressure for where the filling element on feeder 8 reaches minimum fluidisation velocity

It is seen that the valve placement on the cell might be beneficial as the transient phase increases with distance from the valve. Another important factor to address is the reduction in steady state fluidising velocity. As mentioned earlier an over-fluidisation is less controllable and more turbulent than when the fluidisation velocity is closer to minimum fluidisation velocity V_{mf}. Moving the valves to the element does, however, not change the fact that the elements are operating with a high fluidising velocity.

It is also important to note that the previously mentioned measurements does not indicate a lower standard deviation on cell L22 with valves mounted on the feeding elements. This could mean that the transient phase has little or no effect on the standard deviation in dose size. On the other hand, the measurements on cell L22 only consists of one data set (one cycle per feeder) and might not be fully reliable. It is, therefore, important that the functionality of both the feeders and the cell air slide is tested before drawing any conclusions.

Chapter 4

Pressure Reduction on Current Design

4.1 Intention

Based on the results presented in the previous chapter it is theoretically possible to reduce the pressure in both the cell air slide and the point feeders to reduce the total air consumption. The reduction in air consumption is primarily a driving force for the cell air slide as it has a high consumption of compressed air.

The point feeders does, on the other hand, operate with an initially low air consumption and a reduction does, therefore, not have a significant effect on the total operating cost, as previously mentioned. The driving force behind this reduction is to reduce the fluidisation velocity to stabilise the doses. An increased stability in the dose size is expected both due to the fact that they are currently operating with a large fluidisation velocity that could cause turbulence in the alumina flow and the fact that a pressure reduction will increase the time period of steady state fluidising velocity on the element.

To reduce the pressure, a dynamic pressure regulator would be beneficial as it includes an electronic control system that makes sure the supplied pressure stays constant. This way the feeders and the cell air slide would be able to operate without influence from a varying supply pressure above the set value. As these valves are expensive equipment and requires far more work implementing on the test rig the tests was carried out using a manual regulator. A function test of these valves is, therefore, not included in this study but the functionality of the components in the production environment is important to investigate before on cell implementation.

4.2 Testing Equipment

Figure 4.1: Picture taken of the rig used for testing

The tests presented in this paper were carried out on a test rig in Hydro's technology center in Årdal, Norway. The test rig shown in Figure 4.1 consists of a 16.5 meter long air slide equipped with nine conveyor elements and one "pillow" below the supply silo. The rig was also equipped with eight feeders of the same design as placed on L22 shown in Figure 4.2. This implies a design criteria of 18 kg control volume and aeration elements according to Table 4.1. Feeder number eight was, however, subject to a current rebuild. Feeder 1 and feeder 7 has, therefore, been used for testing.

Table 4.1: Area of aeration elements on the point feeder on the test rig

Element	Filling	Feeding
Area [m^2]	0.054	0.013
Nozzle diameter [mm]	1.2	1.2
Air supply diameter [mm]	6	6

Figure 4.2: Model of the point feeder used on the test rig

The nine conveying elements are supplied by a Ø19 mm inner diameter pipe and the dimensions of aeration elements on the cell air slide and the nozzle dimensions for each element is presented in Table 4.2. The element width is as for all the CAS elements 134 mm.

Table 4.2: Dimensions of nozzles and aeration elements in the cell air slide on the test rig

Element	Element length [mm]	Nozzle diameter [mm]	Air supply diameter [mm]
1 (Pillow)	280	1.2	Ø6
2	750	1.6	Ø19
3	1,600	2.2	Ø19
4	2,128	2.5	Ø19
5	2,128	2.5	Ø19
6	2,128	2.5	Ø19
7	2,128	2.5	Ø19
8	2,128	2.5	Ø19
9	2,128	2.5	Ø19
10	1,000	1.8	Ø19

The alumina supply to the cell silo was controlled through a Siemens simatic panel shown in Figure 4.3. The panel had indicators signaling when the buffer silo had to be refilled.

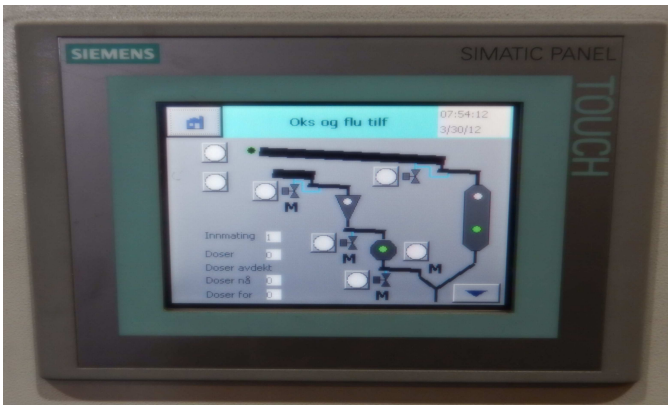

Figure 4.3: Siemens simatic panel used for filling alumina silo supplying the CAS

Input parameters such as number of doses per bin and run time for the feeding element were given as codes to a computer in the cabinet shown in Figure 4.4 and the actual values used will be presented for each specific experiment.

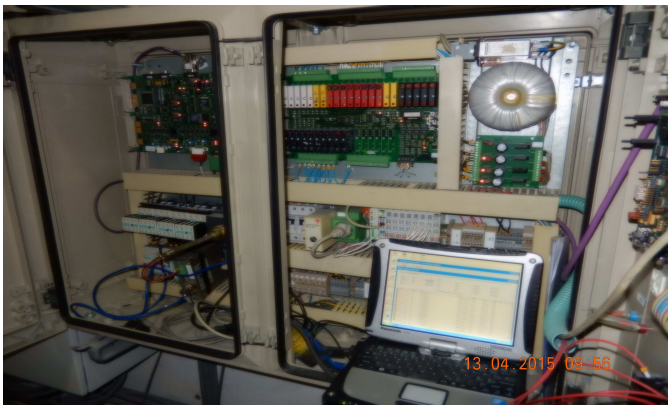

Figure 4.4: Computer used for input of test parameters

The the desired test program was then ran from a cell control cabinet similar to those placed on the actual cells, Figure 4.5.

Figure 4.5: Panel on the control cabinet used to run feeder tests

The final and most important part of the test rig setup was the rebuild of the pneumatic cabinet that was fitted with two pressure regulators. The two regulators allowed the feeders, including the filling and feeding element, and the cell air slide to be operated at different pressure. The regulator valves shown in Figure 4.6 were controlled manually and a pressure gauge on the regulator indicated the adjusted pressure.

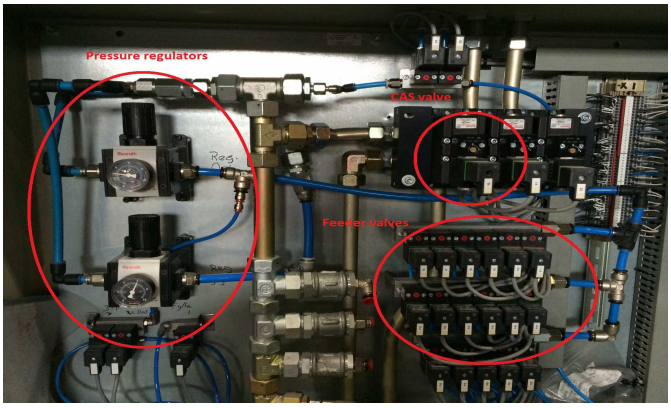

Figure 4.6: Picture of the pneumatic cabinet with the new pressure regulators and the valves controlling each feeder and the cell air slide

A bench scale from Mettler Toledo was use to weigh each dose beneath the element. The scale had a maximum capacity of 15 kg and a readability of 1 gram. The setup with bucket and scale is shown in Figure 4.7.

Figure 4.7: Bench scale and bucket setup for testing

4.3 Simulations of the Test Rig

Due to the test rig air slide operating with nozzles slightly different from those on the actual cells it was important to carry out simulations to show that the slide behaviour is the same as in the operating cells. The test rig design is very similar to the one present on cell L22 and L23 for the cell air slide and an exact copy of the feeder design present on cell L23.

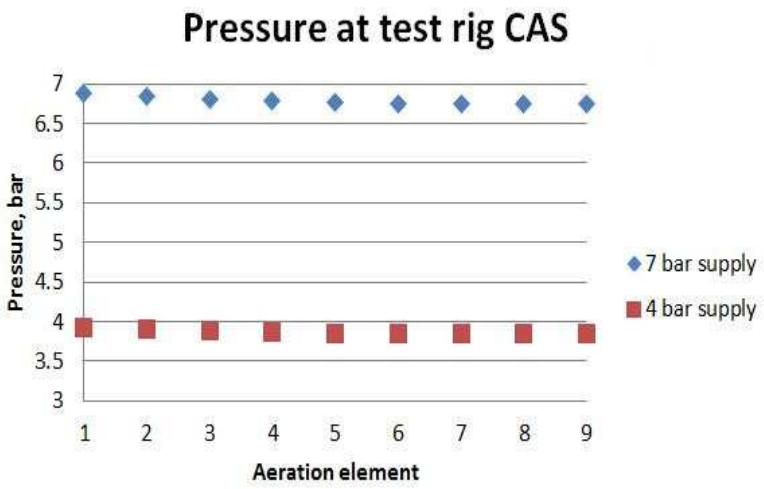

Figure 4.8: Pressure simulations for the cell air slide on the test rig indicating the same low pressure drop as seen in cell L22 and L23 over the elements

Starting with the pressure measurements shown in Figure 4.8 the design shows a low pressure drop over the aeration elements as expected due to the Ø19 mm inner diameter supply pipe. This is similar to the pressure drop observed for CAS design 1 present on cell L22 and L23. The simulations include only the transportation elements 1-9 as done and explained previously.

Table 4.3: Area of aeration elements on CAS on the test rig together with calculated fluidising velocity based on Equation 2.21 and 2.23 V_{0c} and simulated values V_{0s} with 7.0 bar absolute pressure

Element	1	2	3	4	5	6	7	8	9
Area $[m^2]$	0.1005	0.2144	0.2852	0.2852	0.2852	0.2852	0.2852	0.2852	0.1340
V_{0c}	2.07	1.84	1.80	1.79	1.79	1.79	1.79	1.78	1.91
V_{0s}	2.29	2.04	1.98	1.97	1.97	1.96	1.96	1.96	2.15

Moving on to the velocity simulations an important note is that the simulated fluidising velocity is slightly higher than the one calculated from nozzle calculations from Equation 2.21 and 2.23. This means that the simulated fluidising velocity might be slightly higher than the actual fluidising velocity. The results from simulations with 7.0 and 4.0 bar absolute pressure is presented in Figure 4.9.

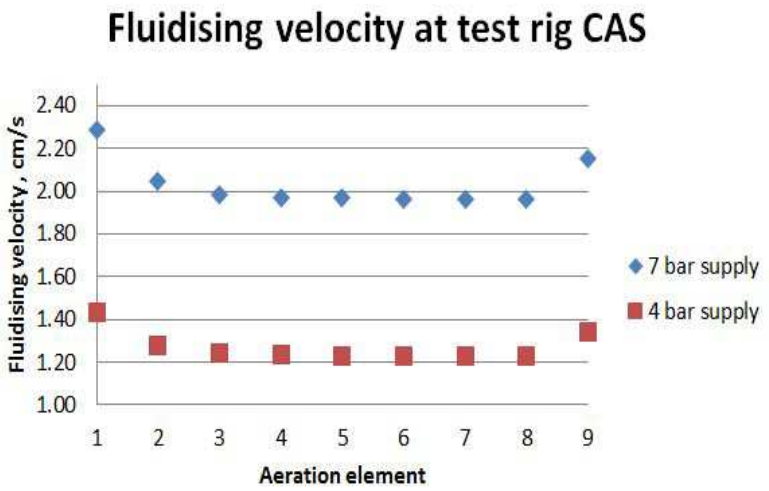

Figure 4.9: Fluidising velocity V_0 based on simulations for the cell air slide on the test rig showing a stable fluidising velocity with peaks on the first and last transportation element

The simulations for the test rig shows similar results as those for design 1 present on cell L22 and L23 with a stable fluidising velocity slightly above 2.0 cm/s for 7.0 bar and about 1.3 cm/s for 4.0 bar absolute pressure.

4.4 Pressure Reduction on Point Feeders (6.0 - 3.0 barg)

Based on simulated results it is believed that it is possible to reduce the air consumption in the point feeders by reducing the supplied air pressure without having an impact on the functionality. The reduction in air consumption and thus fluidising velocity was, however, expected to reduce the transport capacity as explained earlier. The reduction of fluidising velocity was also expected to reduce the standard deviation in the dose sizes due to a decrease in the time period with a transient fluidising velocity according to the simulations presented in Figure 3.23.

The intention of the initial tests was, therefore, to estimate the coherence between the capacity and fluidising velocity in addition to investigating the standard deviation of the doses at different pressures.

4.4.1 Method

First of all, parameters for number of doses and dose time was set. Additionally the test program was set to HAL4e feeders and a 5 second operating time was added to the last dose to make sure the control volume was empty after each cycle. The time parameter set for doses was selected by a short observation of what resulted in doses around 900 g. This resulted in the initial dose time t_{d} being set as shown in Table 4.4. In between each dose a de-fluidisation period of 20 seconds was used, which according to K. Norheim, 2013 [14] is considered to be more than sufficient.

Table 4.4: Initial parameter setup for pressure reduction rest

Feeder number	1	7
Dose time t_{d} [s]	3.4	3.8
Number of doses	21	21

The parameters for CAS and filling element operation was preset with the program interval shown in Figure 4.10 and ran once after every control volume cycle. The reason for the two 1 second pulses before filling of the control volume is to "plug" the bottom of the control volume to avoid alumina pouring straight through (self-feeding).

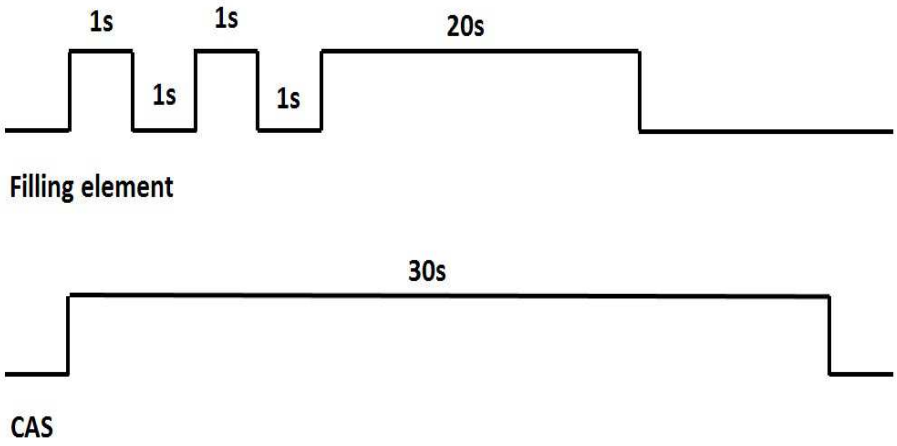

Figure 4.10: Program interval for CAS and filling element of the feeder

The test was then carried out emptying the control volume five times for each pressure as it was reduced with 0.5 bar intervals from 6.0 to 3.0 barg.

4.4.2 Results from Pressure Reduction on Point Feeders (6.0 - 3.0 barg)

In Figure 4.11 the results from the measurements are shown with average dose size for each pressure. It is seen that the first and last two doses are very affected by startup and end effects per cycle. This effect is also present on feeder 7 in Figure 4.13.

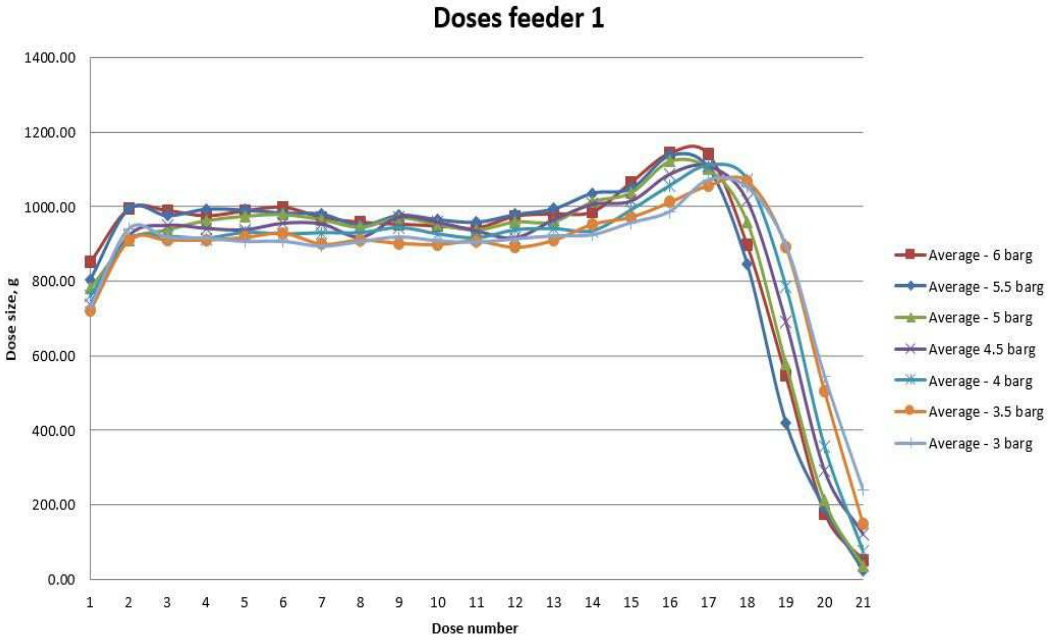

Figure 4.11: Average doses on feeder 1 with reducing pressure

A curiosity on feeder 1 is found at dose 15-19. All tests show an increase in the dose size before the small end effect. The explanation for this could be that the level in the control volume (Figure 4.12) is low enough so that the remaining powder is fluidised resulting in a hydrostatic pressure, Equation 4.1.

$$p = \rho g h \tag{4.1}$$

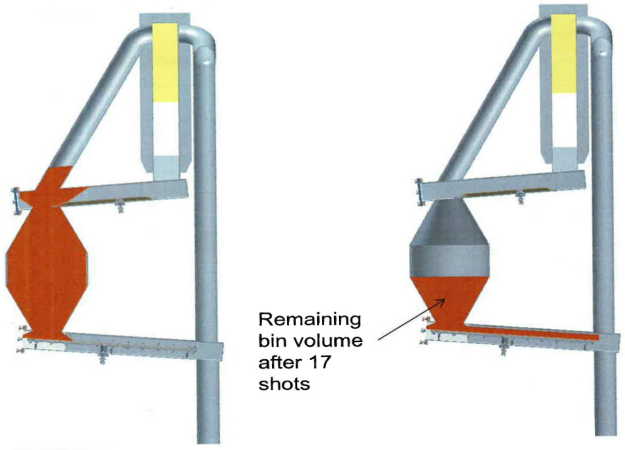

Figure 4.12: Illustration of level variations in the control volume [23]

The problem with this theory is, however, that this effect is not present on feeder 7 seen in Figure 4.13. As the effect was still present in the low pressure operation of feeder one also eliminates the possibility of the difference being caused by a pressure loss from feeder 1 to feeder 7. The dimensions of the apparatus was, therefore, manually measured to find an explanation but no difference was found in either size or de-aeration tube.

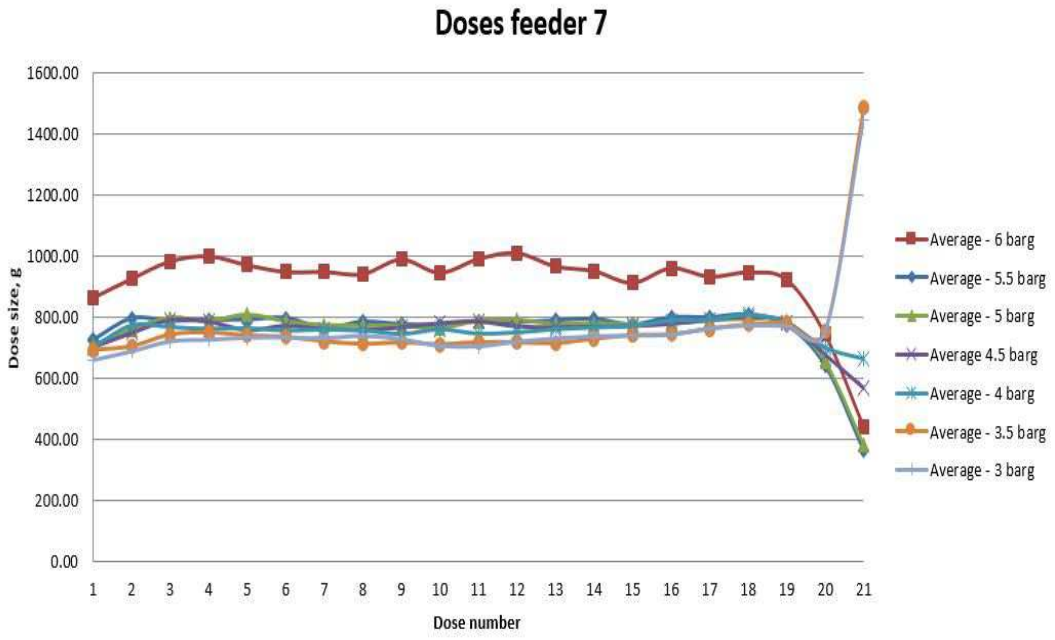

Figure 4.13: Average doses on feeder 7 with reducing pressure

Feeder 7 does on the other hand show another curiosity. As the average dose size is reduced slightly with the reducing pressure this effect is not proportional between 6.0 and 5.5 barg. More measurements was, therefore, carried out on 6.0 barg pressure without any changes in the result and the difference is, therefore, assumed to be real.

It is also possible to notice the startup and end effects on this feeder. The last doses on some of the pressures is as expected high. The reason for this is that the control volume is emptied each cycle and a reduction in the average dose size for the first doses results in an increase in the last dose.

As the control volume is emptied for each cycle the average of all the doses is an irrelevant result for capacity calculations. The results in Table 4.5 and 4.6 is, therefore, calculated without including the startup and end effects. This means that the average doses is calculated from dose 2-19 on feeder 1 and 2-20 on feeder 7.

The total control volume was on the other hand calculated including all the doses. It is, however, a difference in the average control volume size from feeder 1 to feeder 7. This variation is also outside of the internal variations for each feeder. The explanation could, therefore, be a slight change in the alumina quality from the time of the first test to the second. With an apparatus volume of 20.2 dm^3 this results in alumina bulk density ranging between

$902\,\mathrm{kg/m^3} \leq \rho_\mathrm{b} \leq 955\,\mathrm{kg/m^3}$ which are within the normal range. This is by no means a valid calculation of ρ_b due to the unreliable control volume dimensions. The value is calculated purely for explanatory reasons and should not be used for any other purposes.

The positive result is, however, that the average control volume size shows little to no correlation with pressure. This means that, even though a capacity reduction also is expected in the filling element, the run time of the element, Figure 4.10, is sufficient for filling the control volume even at the low fluidising velocities.

Table 4.5: Results from dose measurements on feeder 1

Pressure [barg]	6.0	5.5	5.0	4.5	4.0	3.5	3.0
Average dose [g]	970	963	959	958	948	936	935
STDEV dose [g]	133	154	115	92	76	61	56
RSD dose	13.71 %	15.95 %	12.03 %	9.60 %	8.05 %	6.47 %	6.04 %
Average CV [g]	18,528	18,345	18,292	18,393	18,252	18,223	18,349
STDEV CV [g]	108	84	64	153	20	27	265
RSD CV	0.58 %	0.46 %	0.35 %	0.83 %	0.11 %	0.15 %	1.45 %

Table 4.6: Results from dose measurements on feeder 7

Pressure [barg]	6.0	5.5	5.0	4.5	4.0	3.5	3.0
Average dose [g]	958	933	927	921	913	879	879
STDEV dose [g]	58	55	49	37	36	39	32
RSD dose	6.10 %	5.92 %	5.25 %	3.97 %	3.91 %	4.43 %	3.64 %
Average CV [g]	19,288	18,965	18,852	18,903	18,850	19,027	18,926
STDEV CV [g]	67	99	85	75	40	297	63
RSD CV	0.35 %	0.52 %	0.45 %	0.40 %	0.21 %	1.56 %	0.33 %

The average dose sizes, neglecting the startup and end affected doses, and the dose time t_d was then used to estimate the capacity curve for both feeders presented in Figure 4.14 and 4.15.

$$\mathrm{Capacity}_{\mathrm{Feeder1}} = \dot{m}_{\mathrm{alumina,F1}} = 253.20p^{0.06} \tag{4.2}$$

$$\mathrm{Capacity}_{\mathrm{Feeder7}} = \dot{m}_{\mathrm{alumina,F7}} = 205.19p^{0.11} \tag{4.3}$$

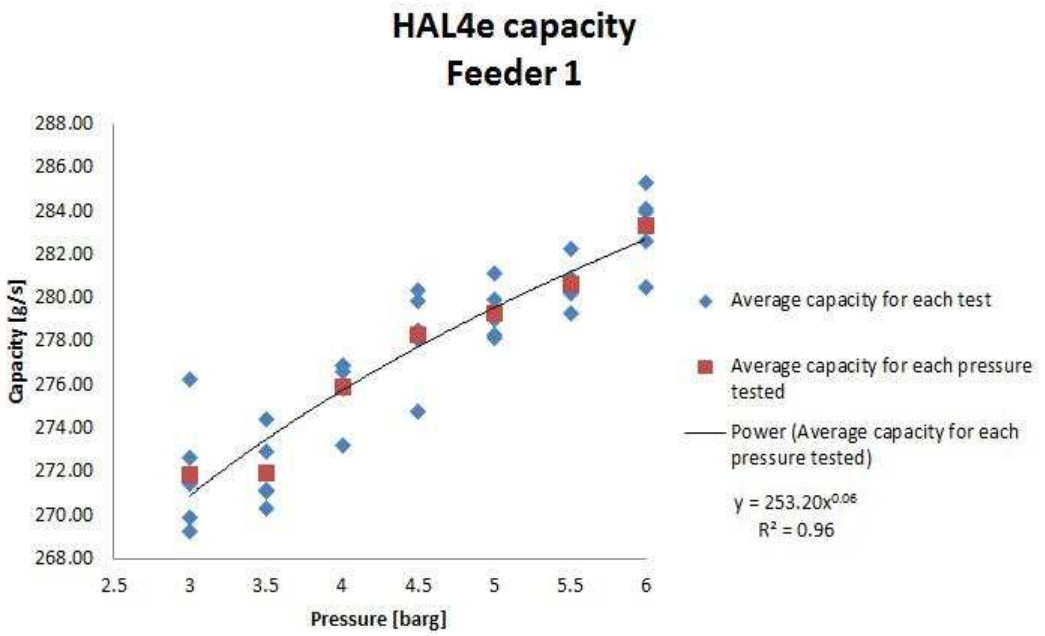

Figure 4.14: Capacity curve fit for feeder 1

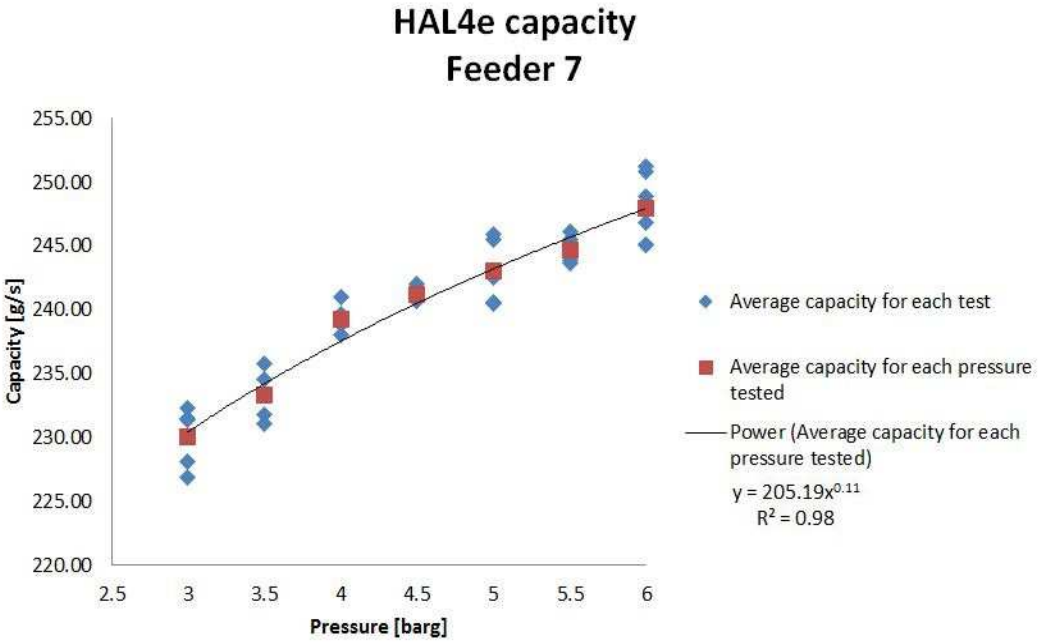

Figure 4.15: Capacity curve fit for feeder 7

The curves in Equation 4.2 and 4.3 was used to estimate new dose times t_{d} which will be explained later. The standardized graphs presented in Figure 4.16 and 4.17 does, however,

show the results as the V_0/V_{mf} ratio after calculation of fluidising velocity with Equation 2.21 and 2.23 and $V_{\text{mf}} = 0.66$, as is used as a Hydro standard [19] [14].

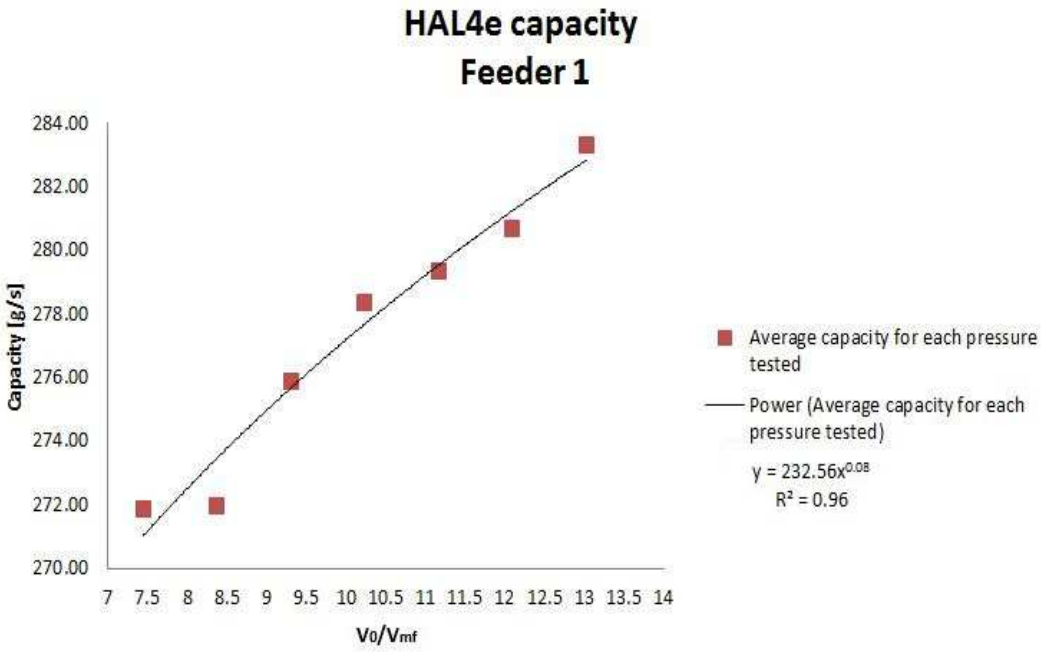

Figure 4.16: Standardized capacity curve fit for feeder 1

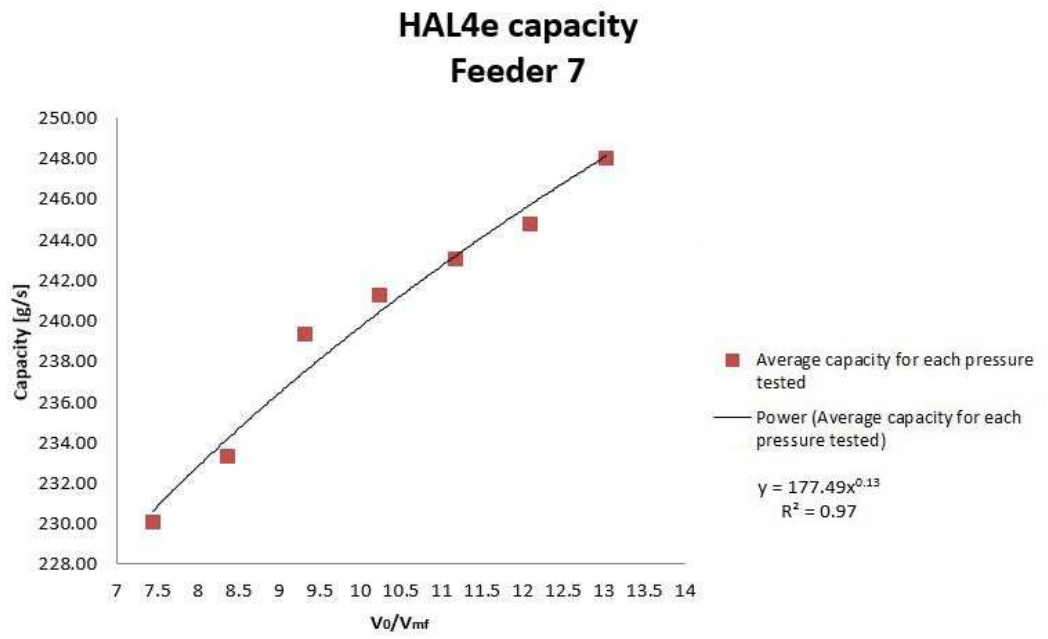

Figure 4.17: Standardized capacity curve fit for feeder 7

It shows that the power curve is a good fit for the measurements with an R^2 value of 0.96 and 0.97 for feeder 1 and feeder 7 respectively. This value is a measurement of how well variations in the data is explained by the curve, Equation 4.4. Ranging from $0 \leq R^2 \leq 1$ the R^2, values of 0.96 and 0.97 indicate a high reliability.

$$R^2 = \frac{\text{Variation}_{\text{explained}}}{\text{Variation}_{\text{total}}} \tag{4.4}$$

A significantly higher capacity on feeder 1 compared to feeder 7 can be observed in the graphs. The theory of a lower bulk density on the material used for testing of feeder 1 is also supported by this result. A material with lower bulk density would, according to the Ergun equation (Equation 2.12) reduce the minimum fluidising velocity and thus increase the capacity. Figure 4.18 illustrates how the minimum fluidisation velocity changes with both bulk density and particle diameter. The relationship between powder quality and capacity is, however, outside the scope of this paper but should be investigated further.

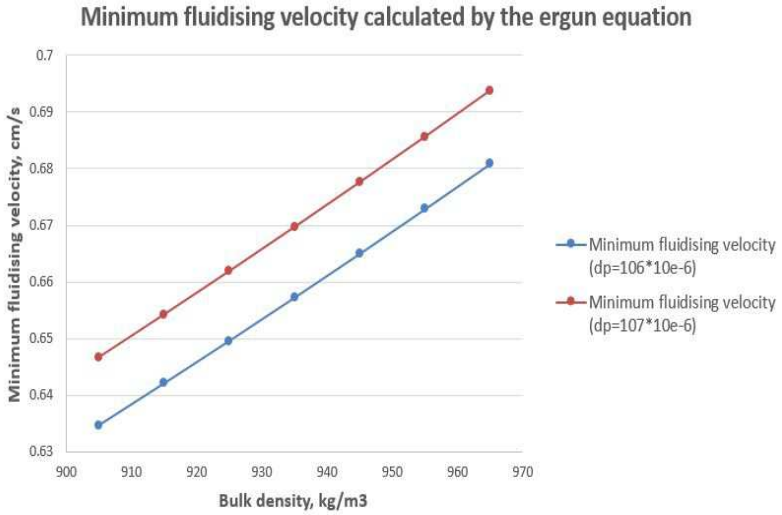

Figure 4.18: Graph illustrating the effect of varying bulk density and particle diameter on V_{mf}

A slight reduction in the relative standard deviation also became present which can also be seen in Figure 4.19 and 4.20. It is, however, some uncertainty related to this due to the deviations in the reduction and more testing was, therefore, required.

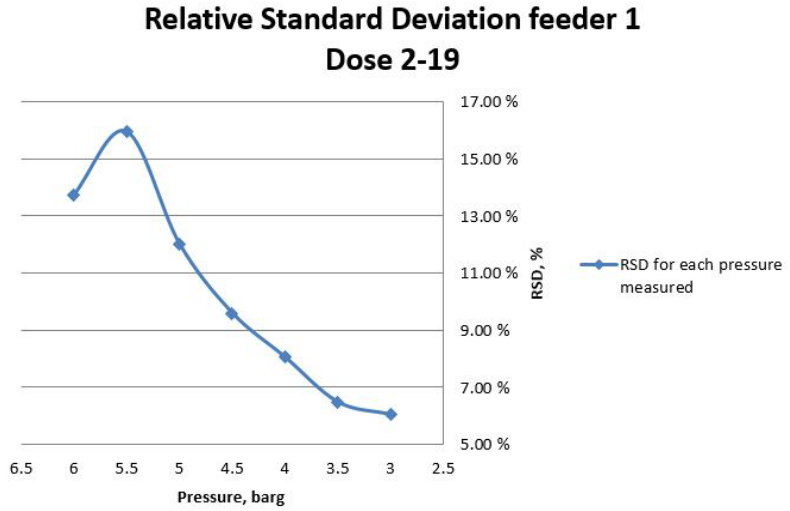

Figure 4.19: Figure showing the reduction in relative standard deviation (RSD) with reduced pressure for feeder 1

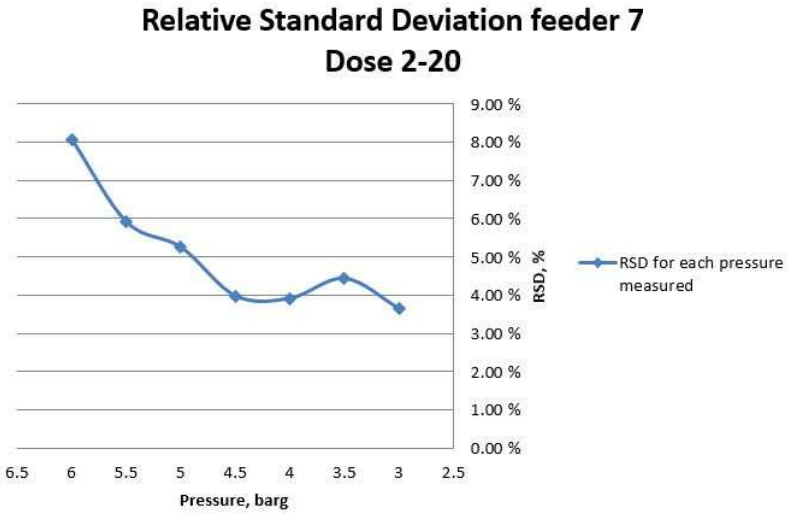

Figure 4.20: Figure showing the reduction in relative standard deviation (RSD) with reduced pressure for feeder 7

4.5 Low Pressure Operation of Feeders (3.0 barg)

With background in the initial results it was seen necessary to do further testing with a low pressure on the feeders. Initial tests proved that the feeders were operational with a low supply pressure and also gave a slight indication that this could reduce the standard deviation in the doses, Figure 4.19 and 4.20. with the intention of further qualification of these results, more tests were carried out with a 3.0 barg pressure.

4.5.1 Method

Based on the previously measured capacity curves in Equation 4.2 and 4.3 the capacity $\dot{m}_{\text{alumina}}$ was calculated for each of the two feeders at 3.0 bar. The average control volume from Table 4.5 and 4.6 at 3.0 bar was divided with 21 doses to estimate the desired dose size m_{dose}. Dosage times t_{d} was then calculated from Equation 4.5.

$$t_{\text{d}} = \frac{m_{\text{dose}}}{\dot{m}_{\text{alumina}}} \tag{4.5}$$

The new parameters are listed in Table 4.7 while remaining parameters were left unchanged. One issue was, however, the fact that the time settings could only be changed with a 0.1 second interval. Some variance from the desired to measured dose size was, therefore, expected.

Table 4.7: New parameters for testing at 3.0 bar

Feeder number	1	7
Desired dose size [g]	874	902
Dose time [t_{d}] [s]	3.2	3.9

To be able to increase the reliability and be able to address the variation in every dose the sample size was increased to 10 control cycles.

4.5.2 Results from Low Pressure Operation of Feeders (3.0 barg)

Initially, this test confirmed the suspicion that the first test of feeder 7 with pressure ranging from 3.0 - 6.0 barg was done with another powder quality as the control volume on the feeders now were in an acceptable range of each other as seen in Table 4.8.

Table 4.8: Table showing the average control volume for both feeders with an acceptable deviation

Feeder number	1	7
Average control volume [g]	18,205	18,463
RSD	0.32 %	0.41 %

As a result of this the calculated time for feeder 7 was to long and a small last dose is, therefore, still present on all the tests with a 3.0 barg pressure as seen in Figure 4.23. On feeder one it is,

however, possible to observe that the reduction in standard deviation for all the doses makes it possible to fine tune the feeding so that the last dose comes within an acceptable range. From Figure 4.21 it is still possible to observe some deviations on the last dose but it shows an improvement from the initial 6.0 barg pressure operation visible in Figure 4.22.

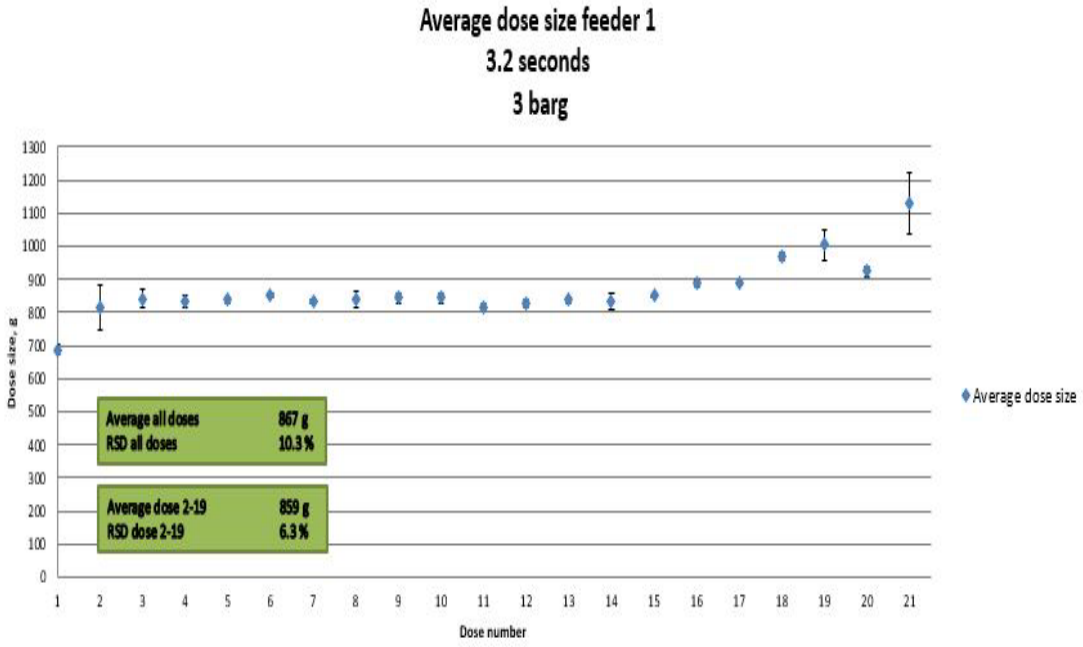

Figure 4.21: Average doses on feeder 1 with 3.0 barg pressure

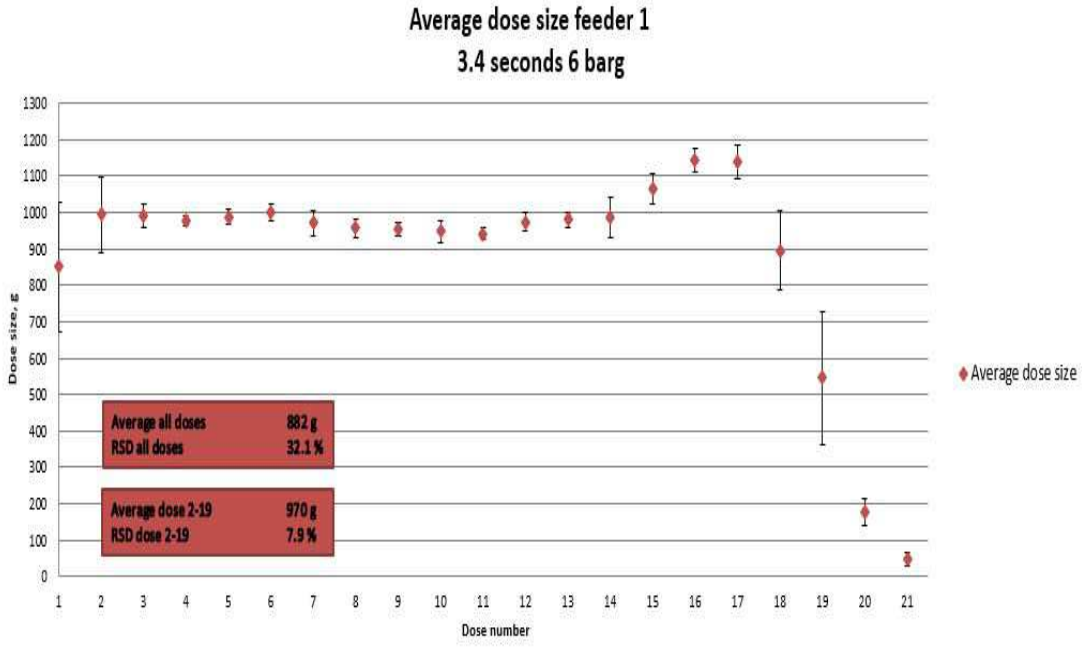

Figure 4.22: Average doses on feeder 1 with 6.0 barg pressure

Due to the alumina quality change from first test on feeder 7 to this test, the doses are not as well tuned as on feeder 1. 3.0 barg pressure on feeder 7 does also show a significant improvement from the 6.0 barg operation as seen in Figure 4.23 and 4.24.

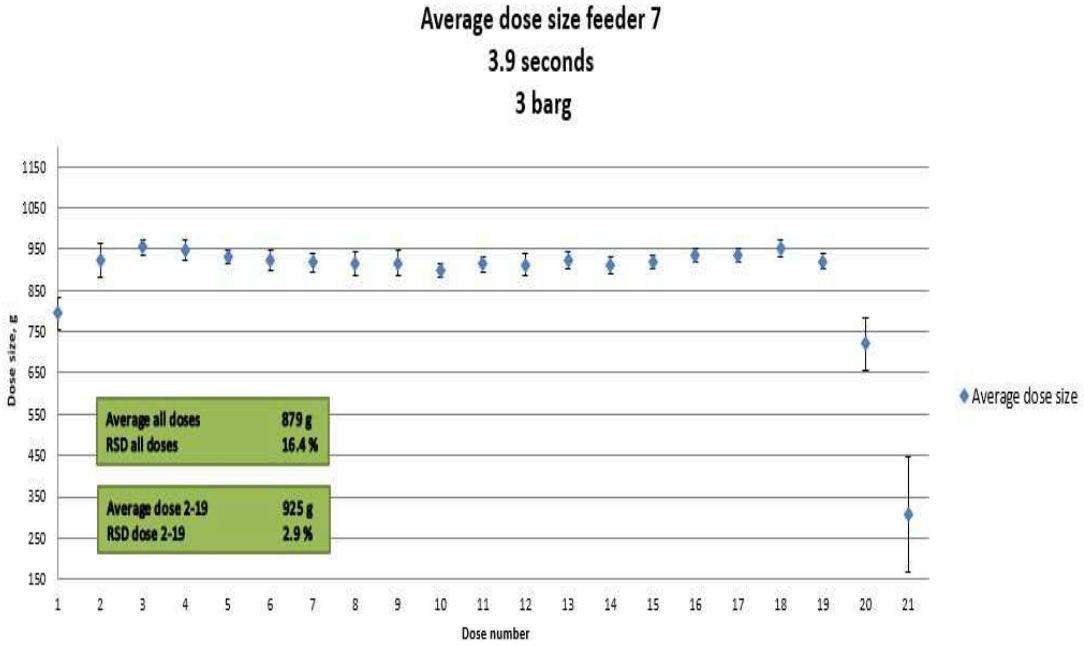

Figure 4.23: Average doses on feeder 7 with 3.0 barg pressure

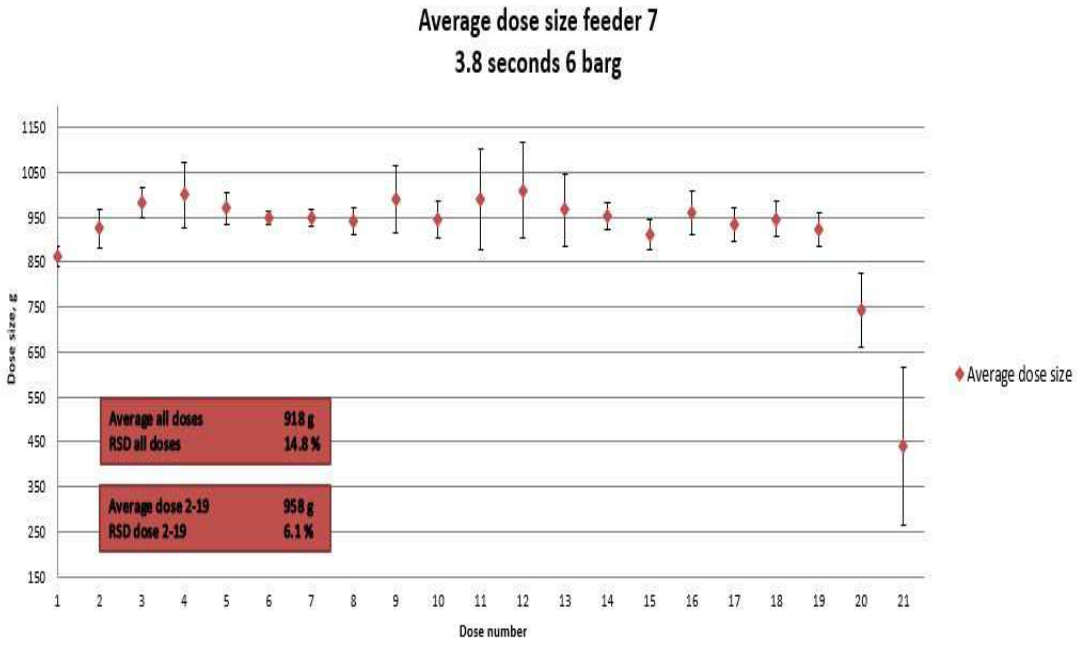

Figure 4.24: Average doses on feeder 7 with 6.0 barg pressure

These tests show positive results when it comes to the standard deviation both on each dose and total control volume. They also indicate that a fine tuning is possible and the last dose effect can be minimized. However, there are still challenges to this fine tuning. First of all it is not possible to operate the valves with an accuracy of more than 0.1 seconds. This means that a perfect tuning might not be possible. Secondly, the last dose will due to current operation with a control volume always be an accumulation of the deviations from dose 1-20. More importantly, the fine tuned process will be very vulnerable to changes in the alumina quality as experienced in the first tests and will, therefore, require extensive testing and calibration for every alumina quality supplied.

4.6 Operation Without Control Volume

From the previous tests it is shown that the pressure reduction on the point feeders has a good effect on the standard deviation on the feeders. Even though this improves the reliability of the doses the fact of the matter is that the deviations due to the startup and end effects are still to high. As a final experiment on the point feeders they have been tested with 15 doses without emptying the control volume each cycle.

The main reason this can be evaluated is that the low pressure operation provides a small deviation in the stable part of the process and could potentially be trusted without the use of a control volume. The control volume has a relative standard deviation of about 0.7 % and to be able to justify the use of a virtual control volume the deviation on the 15 doses should be close to this value.

The theory is that the small first dose is caused by the emptying of the element and the run time on the first dose is too short to fill the whole element and also supply the required dose as shown in Figure 4.25. If this is correct, this effect could be eliminated by not emptying the control volume each cycle.

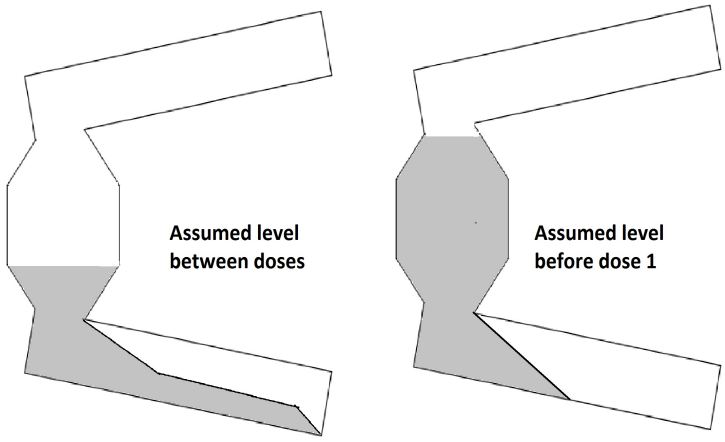

Figure 4.25: Possible explanation for why the first dose is smaller than the rest

4.6.1 Method

This experiment used the same parameters as previously, shown in Table 4.7. To have sufficient data to indicate behaviour on each dose, 10 cycles were taken with the new setting of 15 doses per cycle.

The chosen number of doses were chosen based on the results from Figure 4.21 and 4.23 where it is visible that dose 15 shows no clear end effects.

The procedure was also the same as previously used where all doses were weighed and logged on the bench scale. However, it was important to let the feeder run a full cycle before logging results as it is assumed that the start effects will be reduced.

4.6.2 Results from Operation Without Control Volume

Based on the results presented in Table 4.9 and Figure 4.26 and 4.27 it is possible to conclude that not emptying the control volume has little effect on the first dose. Although a small increase on the first dose average is visible in the table this disproves the hypothesis that this is caused by the emptying the element. This means that the small first dose is a result of the filling of the control volume rather than emptying.

Table 4.9: Table listing the average first dose on both feeders using a 15 and 21 dose cycle

Feeder number	1	7
Average first dose with CV [g]	688.0	794.1
Average first dose without CV [g]	701.6	811.3

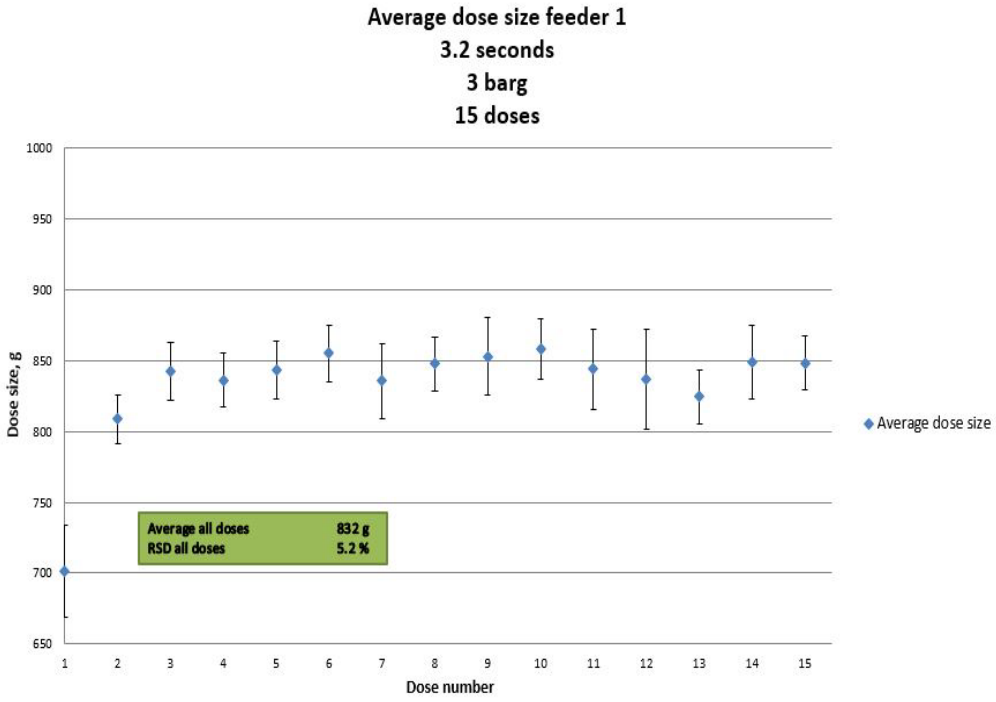

Figure 4.26: Results from 15 doses cycles on feeder 1 without use of control volume

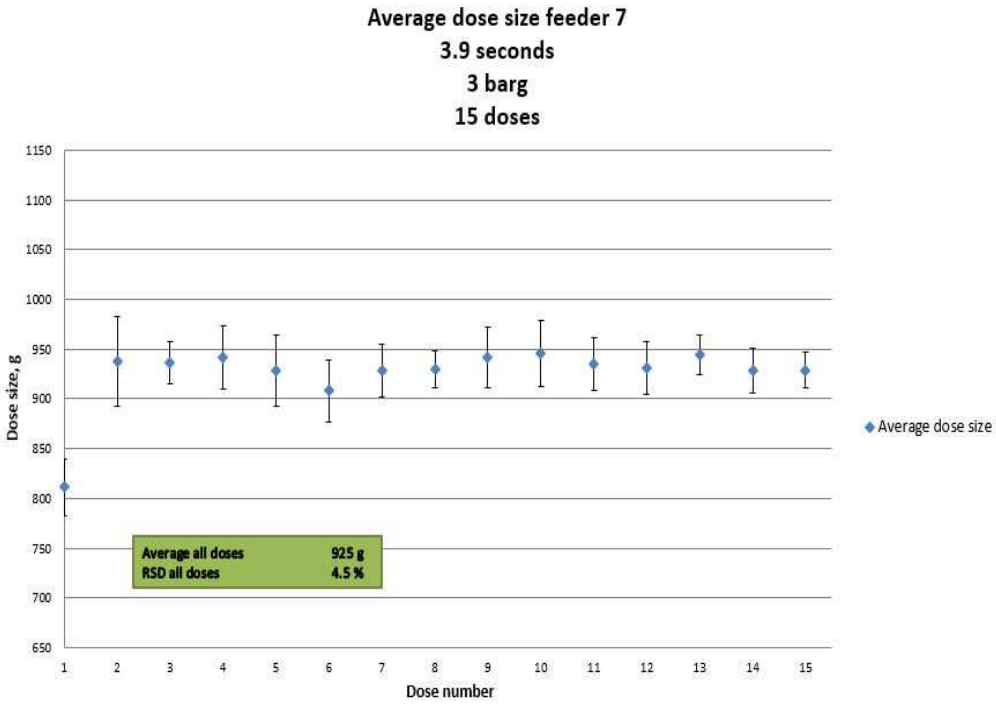

Figure 4.27: Results from 15 doses cycles on feeder 7 without use of control volume

On the positive side these results does show a stable distribution on feeder 1 and 7 with a 5.2 % and 4.5 % relative standard deviation respectively for all doses. This is a significant improvement from the current data presented in 3.12 due to the elimination of the end effects in addition to stabilising the doses with a low pressure.

As mentioned is the use of a control volume important for the cell control as the amount alumina fed to the cell after each cycle is highly reliable even though it results in a high variation in the last doses.

Table 4.10: Reliability of both real and virtual control volume

Feeder number	1	7
Real CV[g]	18,250	18,463
RSD real CV	0.32 %	0.41 %
Virtual CV [g]	12,483	13,878
RSD virtual CV	0.64 %	1.58 %

The results from this experiment shown in Table 4.10 does show that with a low pressure operation at 3.0 barg pressure, the use of a virtual control volume also has a high reliability. Taking feeder 7 as an example this results in a standard deviation of 291.0 g without CV and 75.7 g with CV per 18,463 gram fed to the cell. The question is, therefore, if it is acceptable to do some sacrifices on the long term reliability to achieve a higher reliability in the doses.

Whether it is most important to have reliable doses from dose to dose or long term after 20

doses is a complex question. On one hand the amount of alumina fed to the cell in long term is important for maintaining a stable concentration in the cell. In this case a couple small or large doses have a little effect. A deviation over time can, however, have a larger effect on the alumina concentration in the bath.

On the other hand there is a close monitoring of the alumina concentration through resistance measurements on the cell. As explained earlier and shown in Figure 1.2 the cell voltage would increase if alumina concentration in the cell should deviate from the operational parameters. In the case where this is happening it is important that the feeder can provide reliable doses at that point no matter where in the cycle it is. In the case of too small doses when the cell is "starved" on alumina could result in an anode effect and on the other hand, sludge formation with too large doses when the bath is close to saturation.

4.7 Function Test of Cell Air Slide at 4.5 barg

The current test rig does not allow the same capacity measurements as done for the feeders for different pressures. The experiment was, therefore, a function test based on the previous simulations for 4.5 barg in Figure 3.16. The intention was to investigate weather a reduction in the pressure had any effect in the alumina level in the cell air slide and thus the filling of the control volume. For actual capacity measurements in the cell air slide this report is, therefore, referring to the work conducted by Serena C. Valciu et al. (2014) [21].

4.7.1 Method

The function test was carried out with 10 feeder cycles and the same standard parameters for the air slide as before with a 30 second run time after each feeder cycle. The pressure was reduced to 4.5 barg and the alumina level in the slide was measured as shown in Figure 4.28 above feeder 7 after each of the 10 cycles to investigate whether this stayed constant or was reduced over time. The total alumina mass fed each cycle was also logged to investigate the effect on the feeder unit.

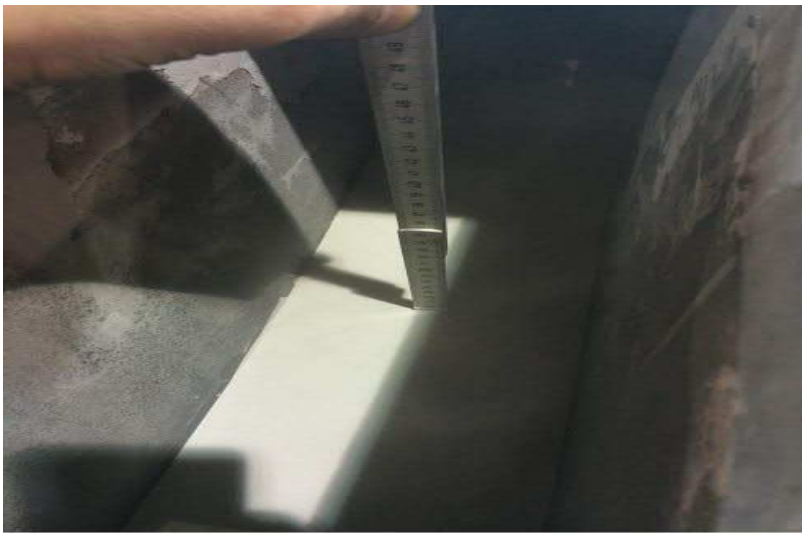

Figure 4.28: Picture of alumina level measurement

4.7.2 Results from Function Test of Cell Air Slide at 4.5 barg

During fluidisation of the cell air slide it was observed that the alumina still reached full bubbling fluidisation with a pressure of 4.5 barg. The measured results shown in Figure 4.29 also indicate that the capacity at 4.5 barg is high enough to reach the steady state bed height in a 30 second interval.

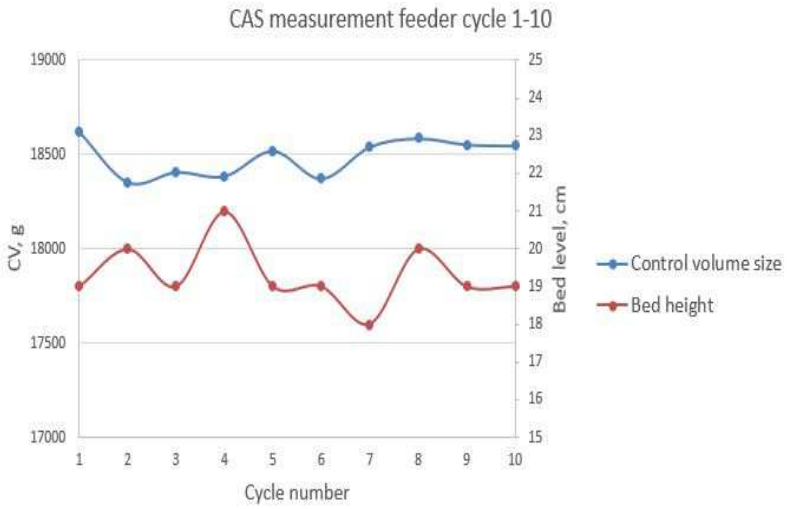

Figure 4.29: CAS measurements for feeder cycle 1-10 after pressure reduction to 4.5 barg

This function test is, however, not reliable on its own. Based on testing with a 1.1° inclined 15 m air slide conducted by Serena C. Valciu et al. (2014) [21], the capacity is reduced to 10 tonns/h at $V_0 = V_{\text{mf}}$ as seen in Figure 4.30.

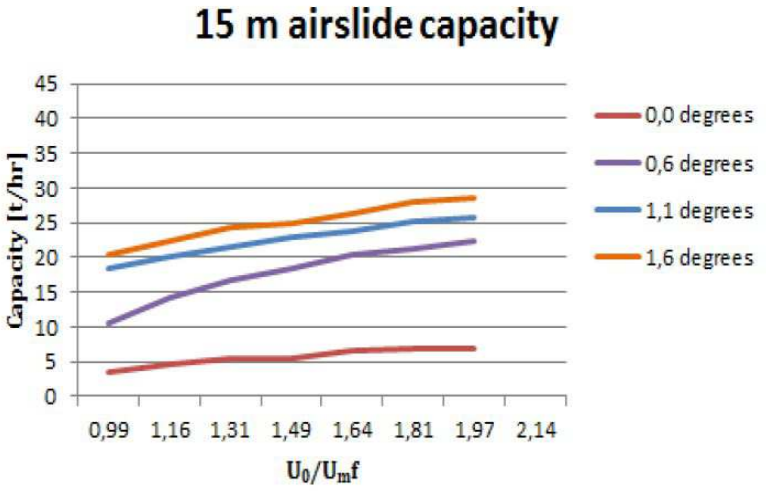

Figure 4.30: Capacity measurements conducted by Serena C. Valciu et. al. (2014) [21]

Based on earlier simulations in Figure 4.9 a 4.0 bar absolute pressure corresponds to a fluidising velocity of $U_0 = 1.2$ cm/s on the dimensioning element. This again corresponds to $\frac{U_0}{U_{\text{mf}}} = 1.76$. Returning to Figure 4.30 this results in a capacity of about 25 tonns/h. On a 30 second interval this is 208 kg which is enough to fill eleven 18.5 kg control volumes. The suggested reduction in fluidising velocity does not have any effect on the alumina level in the cell air slide based on the presented results.

Chapter 5

Conclusions and Further Work

The purpose of this thesis was, as mentioned, to evaluate the current status of the HAL4e alumina distribution system and provide a proposition for improvement of the current design. The conclusion is, therefore, also divided in two parts that will present the optimal design as is today and a suggested solution for improvement of current functionality.

5.1 Current Optimal Design

The issue of current design functionality is divided into two parts to address the cell air slide and point feeders individually. The optimal "current" design is, therefore, not necessarily an actual operating combination on the HAL4e cells. The decision is mainly based on simulated air consumption and fluidising velocity in the air slide and measured dose accuracy for the feeders.

To first address the cell air slide it is seen in Table 3.8 that the design operating on cell L22, L23, L26 and L27 has a much more stable fluidising velocity over the transportation elements than the design currently operating on cell L24 and L25 during optimal conditions (7 bar ABS pressure). This is also seen in the extreme condition (4 bar ABS pressure) in Table 3.9 where one of the elements also operates below the minimum fluidisation velocity of $V_{\text{mf}} = 0.66$ cm/s.

Furthermore, it can be seen in Table 3.10 that the design operating on cell L26 and L27 has an air consumption close to 6% lower than the CAS design on L22 and L23. This is caused by the reduction in supply pipe diameter and the frictional pressure loss that is slightly higher on L26 and L27 which can be observed in Figure 3.10 and 3.14. This pressure loss does, however, not have any effect on the functionality of the current L26/L27design, also in this thesis referred to as design 3. The design is, therefore, evaluated as the optimal design in current production. However, it should be stressed that this is based on current functionality and that the design chosen as the optimal for further development is not the same.

Figure 3.12 presents measurements of the doses on each of the current cells. The only design variation that seem to have an effect is, however, the reduced de-aeration pipe diameter on cell L26 that results in a considerably lower dose accuracy. Other variations do not show consistent results on the dose accuracy and other conclusions can, therefore, not be drawn from the currently available data.

As for the current optimal design this thesis, therefore, concludes that the cell air slide design present on L26 and L27 and the feeders present on all cells except L26 provide good results.

This means that cell L27 is the optimal cell in current production based on the presented data.

5.2 Optimisation of Current Design

For the cell air slide the choice of the optimal design differs from the previous choice. This is due to the pressure loss in the L26 and L27 design explained earlier. For optimisation purposes the L22 and L23 design, also referred to as design 1, is used due to the stable pressure over the cell length.

As seen in Table 3.10, two possible options have been evaluated theoretically with either adjusted nozzles or reduced supply pressure. Based on these simulations and the fact that a pressure reduction provides a more stable fluidising velocity as seen in Figure 3.16, the reduction of supply pressure was considered to be the best option. This is also due to the fact that the initial margin of safety is maintained with a pressure regulator.

A pressure reduction to 5.5 bar absolute pressure was therefore tested on the test rig with the same diameter air supply pipe present on design 1. The current test rig setup did, however, not allow a capacity test of the cell air slide. The test was therefore only a function test where alumina level in the slide and control volume in feeder 7 were measured over 10 air slide cycles after the supply pressure reduction. As seen in Figure 4.29 the results does not indicate any reduction in the alumina level or control volume in feeder 7. This means that the capacity is still high enough to achieve the steady state alumina level in the slide with the current 30 second operating time. This conclusion is also backed by previous measurements on the cell air slide, seen in Figure 4.30, conducted by Serena C. Valciu et al. (2014) [21]. The conclusion is therefore that the supply pressure reduction to 5.5 bar absolute pressure on the cell air slide has no negative sides and that this results in approximately 19% reduction in air consumption.

For the feeders the testing was carried out with the feeder design present on cell L22. In this case the important factor is the dose accuracy as the air consumption is so small that a reduction will have a marginal effect.

The results presented in Figure 4.19 and 4.20 indicate an increased dose accuracy with reducing pressure. It is also shown in Figure 4.14 and 4.15 that the capacity with a 3.0 barg supply pressure is still high enough to supply the desired 900 gram dose within 4.0 seconds.

The low standard deviation in the doses with 3.0 barg pressure can also be observed in Figure 4.21 and 4.23. The main reason for the high total standard deviation is, however, the start and end effects in each cycle which are still present with a 3.0 barg supply. This thesis does therefore present a solution where the feeders operate with 15 doses and thus not emptying the control volume each cycle. The results presented in Figure 4.26 and 4.27 show that this eliminates the end effects as expected. The start effect is still present and is therefore caused by filling of the control volume rather than emptying.

This possible solution can be considered due to the low standard deviation on the doses with a 3.0 barg supply pressure that reduce the need for an actual control volume. There is, however, still a slight increase in the relative standard deviation over time without the use of a control volume as can be seen in Table 4.10. The benefit of stable doses versus stable supply over time has to be evaluated further, even though the marginal increase in RSD over time indicate that not emptying the control volume could be beneficial. Either way, the reduction of pressure in the point feeders result in a reduced standard deviation and should therefore be considered for implementation.

5.3 Further Work

Based on the results presented in this thesis, pressure regulators has been ordered and will be implemented on the HAL4e cells located in Årdal, Norway. This will, therefore, be a small scale industrial functional testing of the presented solution. The testing in a larger scale and over a longer period of time is important to validate the results presented in this thesis before possible implementation in the new Hydro Karmøy HAL4e pilot plant.

This will also validate the functionality of the dynamic pressure regulators in the production environment. A function test is important due to the harsh production environment with dust and strong magnetic fields.

Further more, this thesis does not offer fully reliable data on the effect of pressure reduction on the cell air slide due to the test rig limitations. Even though several measurements on this has been carried out over the years, it is recommended that this is done with the actual present air slide design. This could also uncover the limit or pressure reduction as it is believed that it is believed to be lower than the 4.5 barg solution presented in this thesis.

Finally, it would be beneficial to reduce the effect of alumina quality changes wich is present both in current design and in the suggested optimisation. Determining capacity curves, as done in this thesis might on the other hand be too time consuming to implement on a normal basis. Other possible correlating factors should, therefore, also be investigated so that dose times can be easily adjusted to reduce the effect of alumina changes.

References

[1] K. Grjotheim, H. Kvande *Introduction to Aluminium Electrolysis, Understanding the Hall-Heroult Process*: Aluminium-Verlag, 1993.

[2] H. Kvande, et al. *Pseudo Resistance Curves for Aluminium Cell Control-Alumina Dissolution and Cell Dynamics*: Essential Readings in Light Metals: Aluminum Reduction Technology 1997, p.760-766, 1997.

[3] K. R. Robilliard and B. Rolofs *A Demand Feed Strategy for Aluminium Electrolysis Cells*: Essential Readings in Light Metals: Aluminum Reduction Technology 1989, p.747-751, 1989.

[4] M. Karlsen, et al. *New Aerated Distribution (ADS) and Anti Segregation (ASS) Systems for Alumina*: Essential Readings in Light Metals 2002, p.590-595, 2002.

[5] J. Paepcke, et al. *Startup and Tuning of Material Distribution System at Aluminium Smelter in Qatar*: Essential Readings in Light Metals 2014, p.743-746, 2014.

[6] D. Kunii and O. Levenspiel *Fluidisation engineering Second Edition*: Butterworth- Heinemann, Series in Chemical Engineering, 1991.

[7] D. R. Escudero *Bed height and material density effects on fluidized bed hydrodynamics*: M.Sc. thesis, Iowa State University, 2010.

[8] C.T. Crowe *Multiphase flow handbook*: CRC Press, 2006.

[9] D. Geldart *Types of gas fluidization*: Powder Technology 7(5) p.285-292, 1973.

[10] P. D. S. de Vasconcelos and A. L. A. Mesquita *Gas-Solid Flow Applications for Powder Handling in Industrial Furnaces Operations*: Heat Analysis and Thermodynamic Effects, 2011.

[11] D. C. Sau et al. *Minimum fluidization velocities and maximum bed pressure drops for gas-solid tapered fluidized beds*: Chemical Engineering Journal Vol. 132, 2007.

[12] N. Hilal, M. T. Ghannam, M. Z. Anabtawi *"Effect of bed diameter, distributor and inserts on minimum fluidization velocity*: Chemical Engineering and Technology Vol. 24, 2001.

[13] J. V. Fletcher, M. D. Deo and F. V. Hanson *Fluidization of a multi-sized Group B sand at reduced pressure*: Powder Technology 76 p.141-147, 1993.

[14] K. Norheim *Fluidisation tester*: Internal Hydro report, PMT 009, 2013.

[15] C. Y. Wen, Y. H. Yu *A Generalized Method for Predicting the Minimum Fluidization Velocity*: A.I.Ch.E. p.610, 1966.

[16] P. D. S. de Vasconcelos and A. L. A. Mesquita *Minimum and Full Fluidization Velocity for Alumina Used in the Aluminium Smelter*: INTECH Vol. 3 No. 4 , 2011.

[17] R. Szymkiewicz *Numerical modeling in open channel hydraulics (Vol.83)*: Springer, 2010.

[18] K. Keunecke *Fluidization and fluidized bed conveyance of small-particle-size solids*: VDI Forschungsh, 1965.

[19] S.C. Valciu *Air Slide Basic Modelling*: PhD Thesis, Under Review, University of Greenwich, 2015.

[20] C. E. Agu and B. Lie *Numerical Solution of the Saint Venant Equation for non-Newtonian Fluid*: Proceedings of the 55th Conference on Simulation and Modelling (SIMS 55), 2014.

[21] S.C. Valciu et al. *Mechanical design principles and test results of a small scale airslide rig for alumina transport*: Proceedings from The 55th Conference on Simulation and Modelling (SIMS 55), 2014.

[22] F. M. White *Fluid Mechanics Second edition*: McGraw-Hill Book Company, 1986.

[23] H. Kueppers *HAL4e Feeder, Dose Size raw data*: Data collected as part of commissioning work HAL4e, 2011-2014.

Appendix A

Appendix

A.1 FluidSim Correlation with Empirical Data

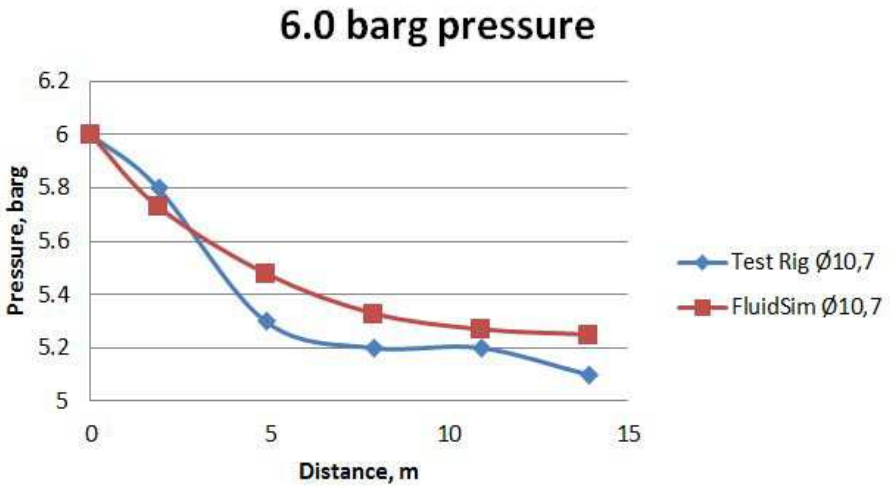

Figure A.1: Comparison of simulated values using FluidSim and measurements from the Porsgrunn test rig at 6.0 barg

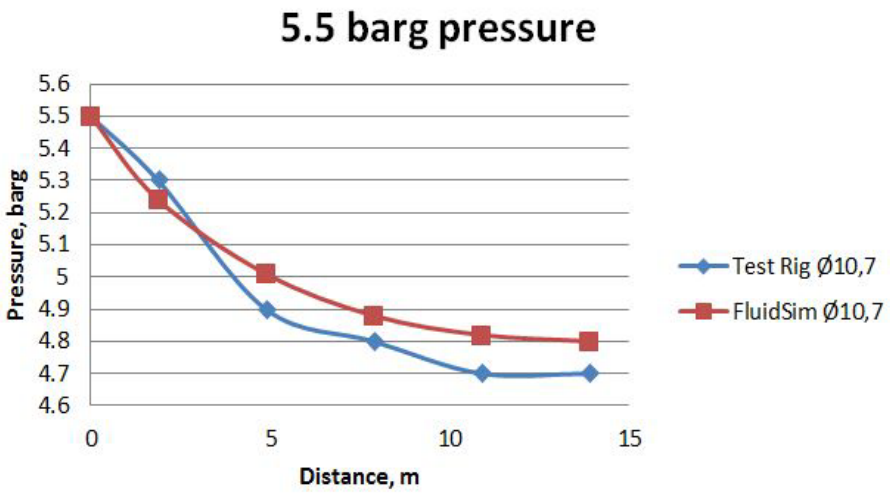

Figure A.2: Comparison of simulated values using FluidSim and measurements from the Porsgrunn test rig at 5.5 barg

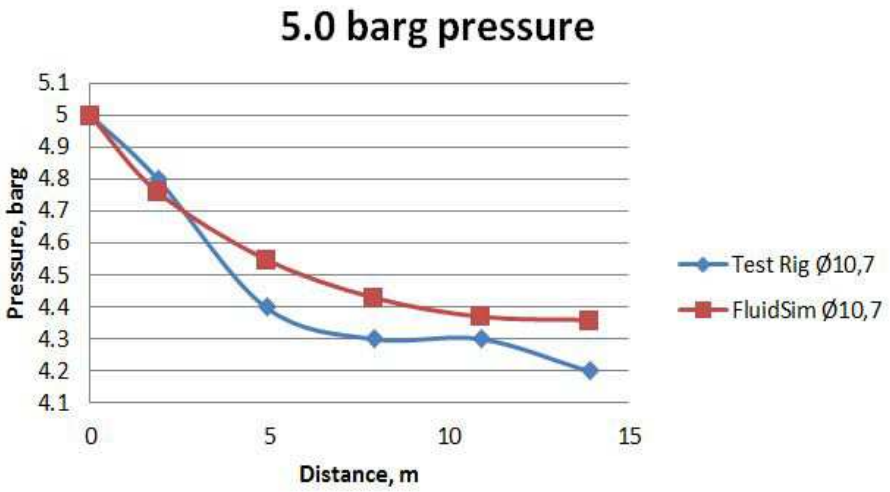

Figure A.3: Comparison of simulated values using FluidSim and measurements from the Porsgrunn test rig at 5.0 barg

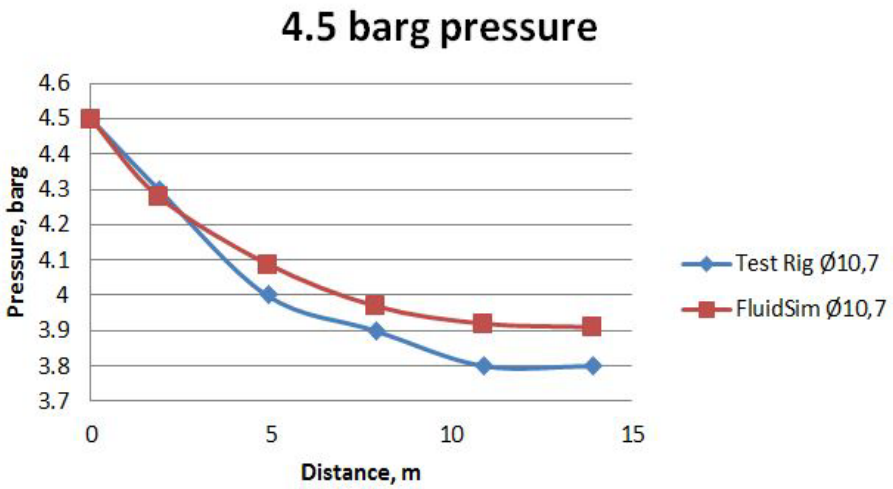

Figure A.4: Comparison of simulated values using FluidSim and measurements from the Porsgrunn test rig at 4.5 barg

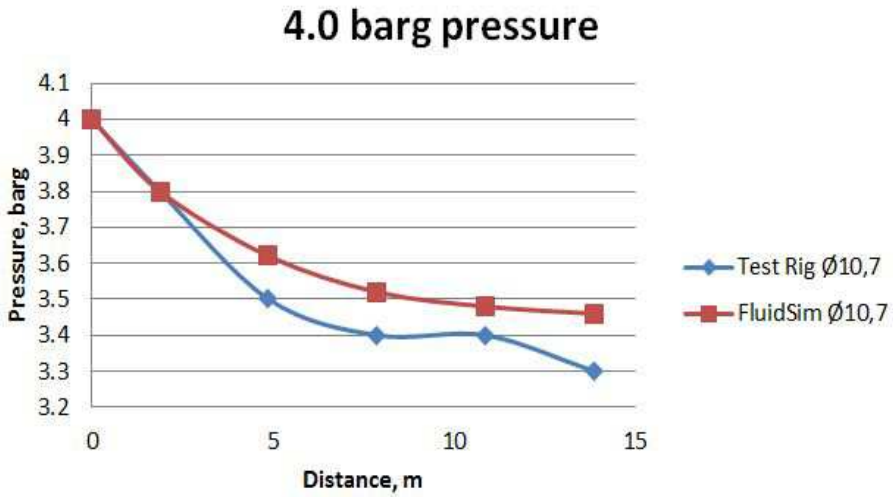

Figure A.5: Comparison of simulated values using FluidSim and measurements from the Porsgrunn test rig at 4.0 barg